Full title

Diversity and functional specialization of oyster immune cells uncovered by integrative single cell level investigations

Short title

"Functional specialization in Oyster's immune cells"

Authors

Sébastien de La Forest Divonne[1], Juliette Pouzadoux[1], Océane Romatif[1], Caroline Montagnani[1], Guillaume Mitta[3], Delphine Destoumieux-Garzon[1], Benjamin Gourbal[2], Guillaume M. Charrière[1#], Emmanuel Vignal[1#*]

Affiliations

[1] IHPE, Univ Montpellier, CNRS, Ifremer, Univ Perpignan Via Domitia, Montpellier, France

[2] IHPE, Univ Montpellier, CNRS, Ifremer, Univ Perpignan Via Domitia, Perpignan, France

[3] Ifremer, IRD, Institut Louis-Malardé, Univ Polynésie française, UMR 241 SECOPOL, 98179 Taravao, Tahiti - Polynésie française, France

* corresponding author: emmanuel.vignal@umontpellier.fr

EV and GC co-supervised the work.

Abstract

Mollusks constitute a large part of the animal biodiversity and play an important role in ecosystems and global food security. The Pacific oyster, *Crassostrea (Magallana) gigas*, is the most farmed bivalve mollusc in the world and has become a model species. Despite the number of studies on bivalves' immune cells, the hemocytes, their characterization remains elusive. By using a combination of single-cell RNA sequencing, quantitative cytology, functional assays and trajectory analyses, we characterized a total of seven distinct hemocyte types and defined at least three hematopoietic lineages. This integrative analysis allowed us to reconcile molecular and cellular data and identify cell types performing specific immune functions such as phagocytosis,

ROS production, copper accumulation, and expression of antimicrobial peptides. These findings pave the way for a deeper understanding of key physiological and immune responses, to help develop mitigation strategies, limit the impact of disease and to contribute to the sustainability of bivalve farming.

Introduction

Mollusca is the second largest invertebrate phylum after Arthropoda, and the largest marine phylum, comprising approximately 23% of all known marine organisms (*1*)**.** Among them, bivalves are highly diverse and display a rich evolutionary history (*2*). The Pacific oyster *Crassostrea (Magallana) gigas* (*C. gigas* - Thunberg, 1793) (NCBI:txid29159) is a sessile filter-feeding bivalve that thrives in a variety of stressful environments ranging from intertidal to deep sea (*3*), and is key species for the aquaculture industry worldwide (*4*). Several infectious diseases affect *C. gigas* at different life stages, impacting its production, and considering its significant socio-economic value, considerable attention has been paid to better understand and to mitigate these diseases (*5*). The causes of these mortalities can involve a variety of pathogens, including viruses, bacteria and parasites that can be responsible for the mortality events affecting *C. gigas* (*6*). One of the most studied infectious diseases to date is the POMS (Pacific Oyster Mortality Syndrome), a polymicrobial disease responsible for mass mortalities of juvenile oysters (*7*). It is triggered by the OsHV-1 µVar herpesvirus, which alters the immune defenses of oysters and allows the colonization of opportunistic bacteria, including *Vibrio*, that cause hemocyte lysis and bacteremia that lead to animal death (*7*). Other bacterial pathogens have also been implicated in mass mortalities of adult Pacific oysters in several countries, and the most emblematic one is *Vibrio aestuarianus* which affects adults in Europe (*8*, *9*). To date, most of the oyster pathogens or opportunistic pathogens that have been characterized in detail have all been found to dampen hemocyte defenses during the pathogenic process, at their own benefit. These include the OsHV-1

µVar herpesvirus (*10*) and virulent *Vibrio* strains of the species *Vibrio crassostreae* and *Vibrio tasmaniensis* (*11*), *Vibrio aestuarianus* and *Vibrio harveyi* (*12*), highlighting the critical role of hemocytes in oyster immunity. Immune-based prophylactic treatments, such as immune-priming and immune-shaping, have emerged as innovative solutions to enhance the natural defenses of oysters against pathogens and increase their survival rate, but the development of such therapies is still hampered by a limited knowledge of the underlying molecular and cellular mechanisms (*13*) (*14*).

Hemocytes have been studied since the 1970s (for review see (*15*)). Hemocytes are known as cellular effectors of the immune system that engage in phagocytosis to engulf and destroy potential pathogens, neutralizing parasites by encapsulation, or preventing pathogen dissemination by cell aggregation and release of extracellular DNA traps (*16*). They also participate in the humoral response by releasing cytokines, antimicrobial peptides, and reactive oxygen species (ROS) to combat the pathogens (*17*). In addition to their role in oyster immunity, hemocytes have been implicated in numerous physiological processes ranging from shell repair (*18*) to wound healing, nutrient transport, and environmental contaminant removal (*19*). Despite this acquired knowledge, hemocytes represent a sum of under-characterized populations of circulating immune cells, and knowledge of lineage ontogeny and functional specialization remains poorly understood due to the lack of an unified classification and of limited molecular and functional genetic tools. Several studies have proposed different classifications of hemocytes in the *Ostreidae* family, with 3 to 4 hemocyte types reported (*15*), all based primarily on either microscopic or flow cytometry analyses. In *C. gigas*, three primary hemocyte cell types have been classically identified : blast, hyalinocyte, and granulocyte cells. While the immune response of *C. gigas* has been extensively studied using classical transcriptomics either at the whole animal, tissue or circulating hemocyte levels, these approaches have ignored the diversity of hemocyte cell types and lineages underpinning these responses (*20*). However, accurately describing the

diversity of these cells, understanding their ontogeny, and delineating cell lineages is still a fundamental requirement for understanding their specific roles. Thanks to the emergence of single-cell RNA sequencing (scRNA-seq) techniques, it is now possible to monitor global gene expression at single-cell resolution with thousands of individual cells in a single experiment. This provides a unique opportunity to overcome these limitations and deepen our understanding of hemocyte diversity and function in bivalves. Recently scRNA-seq was used to provide a first molecular description of hemocyte population in the oyster *Crassotrea hongkongensis* (*21*). However, in the absence of morphological and/or functional characterization studies, the authors were unable to deduce the hemocyte cell types to be matched to the transcriptomic profiles generated by scRNA-seq.

While many transcriptomic analyses have been performed on *C. gigas* hemocytes, none have been performed at the single cell level. Here, we present an integrative study of *C. gigas* hemocyte diversity at the single cell level by combining scRNA-seq from a pathogen free adult oyster combined with cytology, cell fractionation and functional assays to provide a comprehensive transcriptomic, cytological and functional atlas of hemocyte cell types. Our scRNA-seq analyses identified 7 distinct transcriptomic populations and functional annotation revealed distinct populations with specific functions, including phagocytosis, oxidative burst, energetic metabolism, enhanced transcription, translation and cell division. Thanks to quantitative cytology, 7 morphologically distinct hemocyte cell types were identified, which allowed us to reconcile molecular and cytological data. Density gradients were used to separate hemocyte cell types and qPCR or functional assay analyses were performed to validate cell type-specific markers. Using this combination of analysis, we identified 1 type of hyalinocyte, 2 types of blasts and 4 types of granular cells. In addition, we determined cell types performing antimicrobial functions through phagocytosis, ROS production, copper accumulation, and expression of antimicrobial peptides. Finally, trajectory analysis of scRNA-seq data combined with functional analysis revealed distinct

differentiation pathways that may control hemocyte ontology and differentiation processes. Therefore, we propose here a deeper and up-to-date classification of *C. gigas* hemocytes with a more accurate description of the different cell types, their potential ontology and a precise description of their sub-functionalization.

Results

Single-cell RNA sequencing reveals 7 distinct transcriptomic clusters of circulating immune cells in oysters.

Oysters are known to express a high degree of individual genetic polymorphism, including Copy Number Variation (CNV) or the Presence Absence Variation (PAV) (*22*). Therefore, to avoid misinterpretation of the single-cell transcriptomic data, and to characterize the hemocyte cell types and their heterogeneity, we sampled hemocytes from a unique pathogen free animal (Ifremer Standardized Animal, 18 month-old) and applied single-cell drop-seq technology to 3,000 single hemocytes (**Fig. 1A**). The scRNA-seq library was generated and sequenced, resulting in 127,959,215 high-quality filtered reads available for single-cell analysis (ENA project accession number PRJEB74031). Primary bioinformatics was performed using the STAR solo aligner software (*23*) against the *C. gigas* genome (Genbank reference GCA_902806645.1) from the Roslin Institute (*24*). Out of 127,959,215 reads, 97% showed a valid barcode and 89.2% were mapped to the genome with a saturation of 75.6%. A total of 2,937 cells were profiled, yielding a median of 1,578 genes and 4,412 unique molecular identifiers (UMIs) per cell among the 23,841 total genes detected, with a sequencing saturation of 75.6% (**Supp. Table 1**). For secondary bioinformatic data processing, the Seurat R package (version 4.3.0) was used (*25*). To remove data corresponding to empty droplets or cell doublets, the data set was filtered. Cells with a gene number between 750 and 4,000 and with less than 5% mitochondrial genes were retained. After quality control processing 120 cells corresponding to empty droplets and cell doublets were removed and 2,817 cells were processed for data normalization. Finally, linear dimensional

reduction and clustering was performed on the 3,000 most variable genes from 2,817 cells (**Supp. Fig. S1**). Dimension reduction and clustering led to the identification of 7 transcriptomic clusters in which hemocytes were distributed. These 7 different clusters represented 27.6, 23.1, 17.8, 16.9, 7, 4.6 and 3% of the total cells (**Fig. 1B**). For each transcriptomic cluster, a pattern of over- and under-represented transcripts in each cell was identified (**Fig. 1C**). Average Log2FC values and percentage of expression in each cluster relative to all other clusters were calculated for the Top 10 differentially expressed genes (**Fig. 1D** and **Table 1)**. Clear transcriptomic cell clusters were evidenced as well as specific gene markers for each cluster **(Supp. Data 1**). Only cluster 4 transcriptomic signature was less contrasting than that of other clusters (**Fig. 1D**).

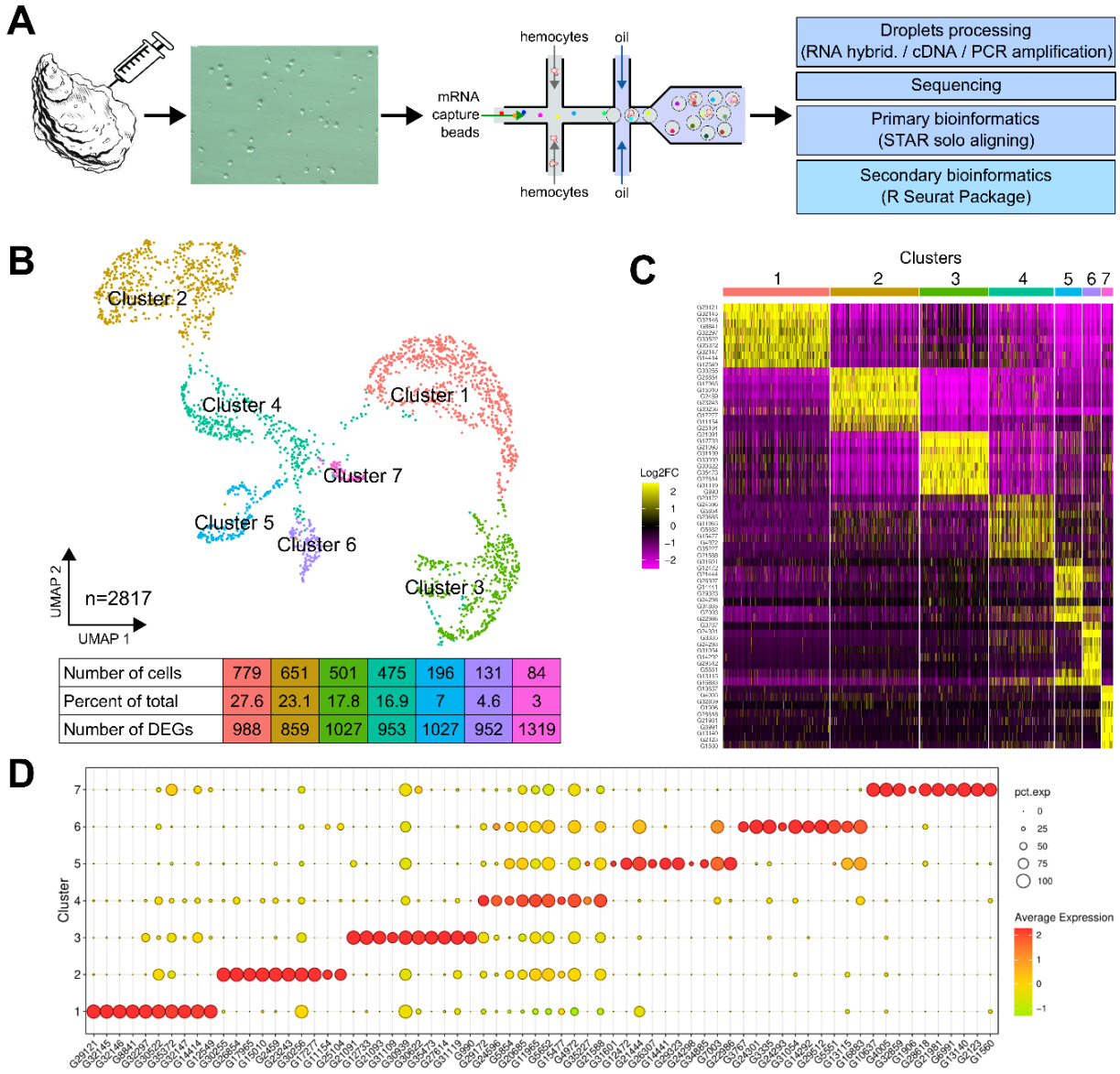

Number of cells	779	651	501	475	196	131	84
Percent of total	27.6	23.1	17.8	16.9	7	4.6	3
Number of DEGs	988	859	1027	953	1027	952	1319

Fig. 1. scRNA-seq analysis of *C. gigas* circulating hemocytes reveals 7 transcriptomic cell clusters (A) Schematic of the scRNA-seq 10X Genomics Chromium microfluidic technology and bioinformatics processing workflow used. Dissociated hemocytes were sampled from a pathogen-free oyster and encapsulated in droplets for processing. After sequencing, the data were processed bioinformatically. **(B)** Uniform Manifold Approximation and Projection (UMAP) plot for dimensional reduction of the data set and summary of the cells and the number of Differentially Expressed Genes (DEGs) in each cluster. The table displays the characteristics (number of cells, percentage of total cells and number of Differentially Expressed Genes in each cluster) of the seven clusters identified. **(C)** Heatmap showing the top 10 overexpressed genes in each cell per

cluster as determined by *FindAllMarkers()* function in Seurat, corresponding to clusters in UMAP plots from **Fig. 1B**, ranked by log2FC. **(D)** Dot plot representing the top ten DEGs enriched per cluster based on average expression (avg_log2FC). Color gradient of the dot represents the expression level, while the size represents the percentage of cells expressing any gene per cluster.

Gene	log2FC	Pct 1	Pct 2	Description
				Cluster 1
G29121	4.31	1	0.099	L-galactono-gamma-lactone oxidase
G32145	4.18	0.992	0.079	Angiopoietin-1 receptor
G32146	3.90	0.985	0.063	Angiopoietin-1 receptor
G8841	3.13	0.988	0.049	C-type lectin domain-containing protein
G32297	2.88	0.99	0.232	PNPLA domain-containing protein
G30522	2.76	1	0.515	Cytochrome P450 2D28
G35372	2.69	1	0.483	60S ribosomal protein L26
G32147	2.45	0.969	0.131	Angiopoietin-1 receptor
G14414	2.45	1	0.343	DUF4773 domain-containing protein
G12549	2.38	0.974	0.132	Glutaredoxin domain-containing protein
				Cluster 2
G30255	5.31	1	0.15	Metalloproteinase inhibitor 3
G26854	4.24	1	0.16	Stanniocalcin
G17965	4.21	0.94	0.04	Complement C1q-like protein 2
G15010	3.99	0.99	0.17	Kyphoscoliosis peptidase
G2459	3.82	1	0.21	*Uncharacterized protein*
G23243	3.51	0.98	0.07	Fibronectin type-III domain-containing protein
G30256	3.23	1	0.69	NTR domain-containing protein
G17277	3.21	0.99	0.04	Putative modulator of levamisole receptor-1
G11154	3.16	0.68	0.05	Collagen alpha-1(XII) chain
G25104	3.1	0.84	0.08	C1q domain-containing protein
				Cluster 3
G21091	5.51	0.99	0.13	X-box binding protein-like protein
G12733	5.42	1	0.12	Galectin
G21093	5.17	0.94	0.05	IgG
G31109	4.36	0.77	0.03	Cystatin domain-containing protein
G30939	4.25	1	0.86	Peptide ABC transporter permease
G30622	3.95	1	0.21	BHLH domain-containing protein
G35473	3.86	0.96	0.04	*Uncharacterized protein*
G27614	3.78	0.96	0.13	G Protein Receptor F1-2 domain-containing protein
G31119	3.77	0.99	0.42	Arrestin C domain-containing protein
G990	3.6	0.93	0.03	LITAF domain-containing protein
				Cluster 4
G29172	3.09	0.78	0.49	G Protein Receptor F1-2 domain-containing protein
G24596	2.37	0.78	0.25	High mobility group protein DSP1
G5854	1.8	0.64	0.38	N-acetyltransferase domain-containing protein
G20685	1.59	0.88	0.53	Ribosomal protein L22
G11965	1.57	0.92	0.7	Ribosome L4 associated C domain-containing protein
G5652	1.54	0.97	0.75	60S ribosomal protein L30
G15477	1.52	0.55	0.3	Metalloendopeptidase
G4972	1.49	0.96	0.8	60S ribosomal protein L12
G35227	1.46	0.55	0.06	ML domain-containing protein
G21588	1.42	0.94	0.69	60S ribosomal protein L13

Gene	log2FC	Pct 1	Pct 2	Description
				Cluster 5
G31601	5.24	0.38	0.06	Polyribonucleotide nucleotidyltransferase
G12472	3.99	0.85	0.03	Galectin
G21444	3.58	1	0.41	*Uncharacterized protein*
G26307	3.42	0.6	0.02	*Uncharacterized protein*
G14441	3.35	0.84	0.08	CUBN
G29323	3.21	0.9	0.01	GTPase IMAP family member 4
G24298	3.18	0.29	0.05	Putative Transmembrane protease serine 9
G34885	3.13	0.59	0.01	Gliding motility-associated C-terminal domain-containing protein
G7003	2.55	0.99	0.16	ETS-related transcription factor Elf-4
G22986	2.37	0.94	0.1	Metalloendopeptidase
				Cluster 6
G3767	6.45	0.74	0.02	Natterin-1
G24301	6.16	0.99	0.02	Aspartate-semialdehyde dehydrogenase
G3335	5.19	1	0.16	*ncRNA*
G24293	4.57	0.59	0.01	*Uncharacterized protein*
G31054	3.56	1	0.13	GATA-binding factor 3
G14292	3.29	0.87	0.03	Membrane-associated guanylate kinase inverted 3
G29512	3.2	0.99	0	Caveolin
G5551	2.93	0.97	0.02	Neuronal acetylcholine receptor subunit alpha-6
G13115	2.73	0.83	0.26	*ncRNA*
G16883	2.62	1	0.2	Allograft inflammatory factor
				Cluster 7
G10637	4.21	0.99	0.03	BZIP domain-containing protein
G4005	4.07	0.99	0.21	Ras-related protein Rab-20
G32859	3.9	0.93	0.04	G Protein Receptor F1-2 domain-containing protein
G1906	3.82	0.5	0.02	Glutathione peroxidase
G28618	3.53	0.91	0.09	Sporozoite and liver stage asparagine-rich protein
G21981	3.5	0.94	0.05	*ncRNA*
G6991	3.4	0.85	0.01	Rho-GAP domain-containing protein
G13140	3.12	1	0.03	DBH-like monooxygenase protein 1
G2123	3.05	0.94	0.02	SPRY domain-containing SOCS box protein 3
G1560	3.02	0.95	0.17	Glutathione peroxidase

Table 1. Top 10 overexpressed genes identified in each transcriptomic cluster. The first column gives the gene number according to the annotation. 'log2FC' represents the log2 fold change of the gene in the cluster compared to all other cells. 'Pct1' is the percentage of cells expressing the gene in the cluster and 'Pct2' is the fraction of cells expressing the gene in all other clusters. Description is the annotation of the expressed gene.

KEGG pathways and GO-terms analyses unveil functional diversity in *C. gigas* hemocytes

ScRNA-seq data evidenced specific functions carried by hemocyte cell types composing the seven transcriptomic clusters. A first global view of the functions over-represented in each cluster

was obtained through a KEGG pathway analysis on the overrepresented transcripts (Log2FC > 0.25) using the *C. gigas* annotation provided by the DAVID consortium (*26*), thereby identifying pathways specifically enriched in each cluster. Cluster 1 was enriched in viral processing and endocytosis (**Figure 2A** and **Supplemental Table S2**). It was also enriched in pyruvate metabolism, glycolysis/gluconeogenesis and pentose phosphate pathways. Clusters 1 and 3 showed a specific enrichment in carbohydrate metabolism and endocytosis. Particularly, cluster 3 was enriched transcripts implicated in glycolysis/gluconeogenesis and TCA cycle activities. Cluster 4 was enriched in protein synthesis, including transcription (spliceosome, ribosome, nucleocytoplasmic transport and mRNA surveillance pathway) folding, sorting and degradation of protein pathways. Clusters 2, 5 and 6 shared a common signature of enrichment in ribosome-related genes, while cluster 2 was specifically enriched in motor protein-coding genes responsible for cell motility and xenobiotic metabolism. Remarkably, clusters 1, 3, 4 and 5 were enriched in oxidative phosphorylation transcripts, whereas cluster 7 was enriched in vesicular trafficking and endo-lysosomal pathways (endocytosis, endosome, phagosome, lysosome, auto and mitophagy).

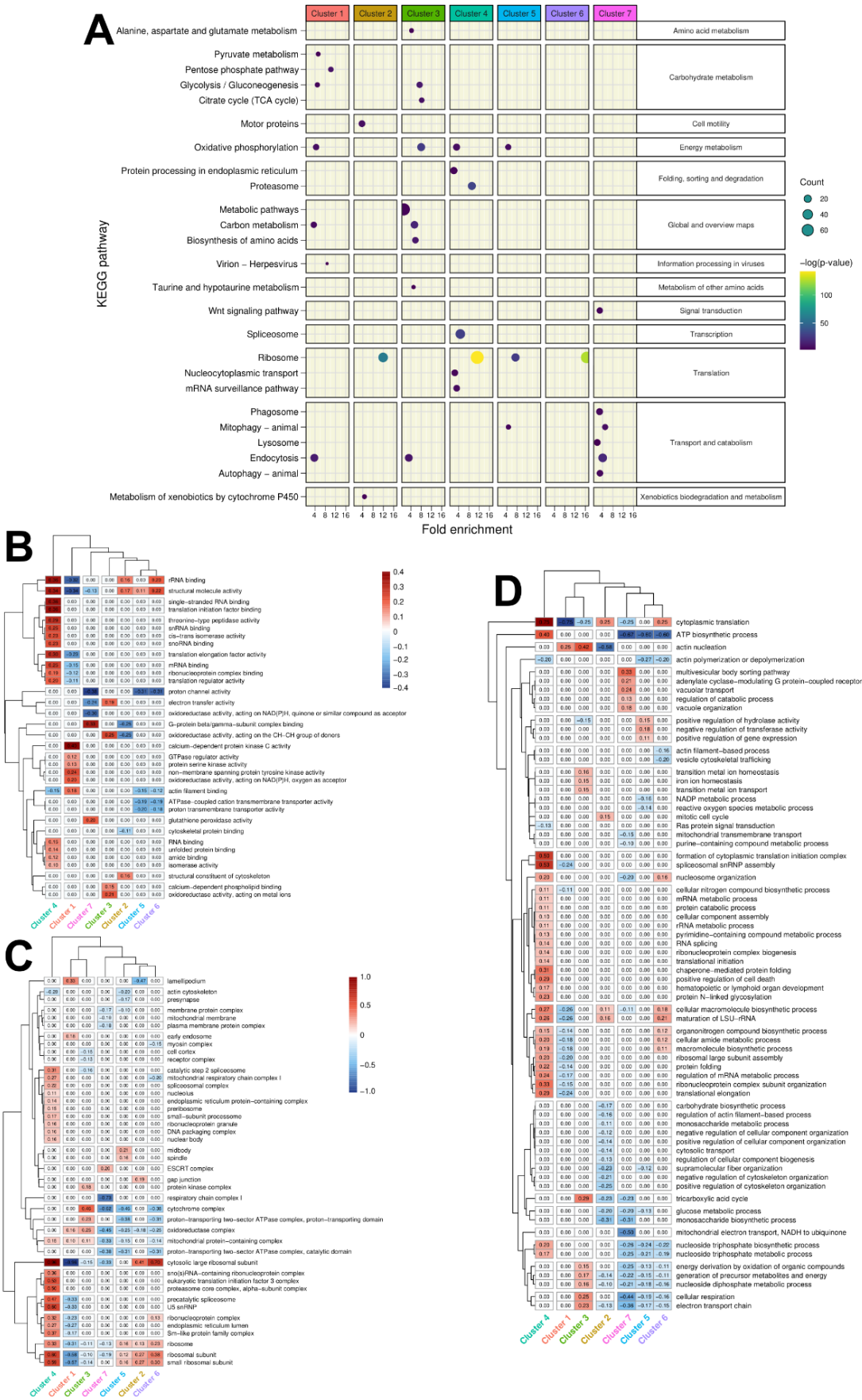

Fig. 2. KEGG and Gene Ontology analysis of the gene signature in each cluster. (A) A synthetic representation of the KEGG pathway analysis is shown. Colored columns represent the 7 transcriptomic clusters. Each row is a KEGG pathway, the colored dot represents the -log(p-value) and the dot size represents the number (count) of enriched genes in each pathway category. The fold enrichment is shown on the x-axis. Panels **(B), (C)** and **(D)** show the results of Gene Ontology terms (GO-terms) for Biological Processes (BP), Cellular Components (CC) and Molecular Functions (MF) respectively, obtained with the overexpressed genes of each cluster (Absolute value Log2FC > 0.25 and significant p-value < 0.001) using RBGOA analysis (p-value <= 0.001) for three different ontology universes. Each panel corresponds to one ontology universe, and the analysis highlights over- and under-enriched terms. The number in the heatmap and the scale indicate the proportion of significant positive GO-terms. Positive values indicate over-enrichment and negative values indicate under-enrichment of the respective BP, CC and MF ontologies.

To delve deeper into the functional characterization of each transcriptomic cluster, we performed a re-annotation of the *C. gigas* genome using a combination of tools to increase the GO term richness of the current annotation prior to functional GO term analysis. For this purpose, we used the *C. gigas* genome (Genbank reference GCA_902806645.1) and the associated gff3 annotation file from the Roslin Institute (*27*). Using these files, the longest CDSs were extracted and processed for GO-term annotation using the Orson pipeline (see Materials and methods). Of the 30,724 CDSs extracted, 22,462 CDSs were annotated (GO-terms and sequence description), resulting in an annotation percentage of 73.1%. Of the 30,724 CDSs, 22,391 were annotated with Molecular Functions (MF), Biological Processes (BP), and Cellular Components (CC) GO-terms (**Supp. Fig. S2 and Supp. Data 2**). Using the GO-term annotation and the Log2FC of genes calculated after scRNA-seq processing in each cluster, GO enrichment analysis was performed by

198 a rank-based gene ontology analysis (RBGOA) (*28*). RBGOA analysis was performed on GO-
199 terms identified in each cluster (**Supp. Data 3**). Results are shown in **Figures 2B, C and D**.
200
201 Overall, scRNA-seq-based analysis identified seven distinct transcriptomic profiles for each cell
202 cluster, shedding light on greater heterogeneity and functional diversity of *C. gigas* hemocytes
203 than previously described. Cluster 1, encompassing 27.6 % of cells, is characterized by
204 morphology and actin cytoskeleton remodeling capacity and oxidoreductase activity, as indicated
205 by an enrichment in oxidoreductase activity acting on NAD(P)H and kinase activities BP, actin
206 nucleation MF and lamellipodium and early endosomes CC. Cluster 2, comprising 23.1 % of
207 cells, has an increased translation activity, as indicated by enrichment in BP, MF and CC terms
208 related to rRNA binding, cytoplasmic translation, maturation of LSU-rRNA, and ribosomes
209 respectively. Cluster 3, making up 17.8 % of cells, shows enrichment in cellular oxidation and
210 actin nucleation, as indicated by an enrichment in BP and MF related to oxidoreductase activities
211 acting on metal ions, electron transfer, cellular oxidation and actin nucleation, and CC related to
212 cytochromes, oxidoreductase complex, and mitochondrial protein-containing complexes. Cluster
213 4, include 16.9 % of the cells, has transcriptomic signatures reminiscent of spliceosome assembly,
214 rRNA maturation, and ATP biosynthesis (BP related to RNA binding, translation, and
215 proteasome, MF related to spliceosome assembly, rRNA maturation, and ATP biosynthesis, and
216 CC related to nuclear bodies and ribosomes). Cluster 5, with 7 % of cells, shows enrichment in
217 structural molecule activity, hydrolase regulation, and gene expression, evident in its BP, MF, and
218 CC related to ribosome, midbody and spindle localization. Cluster 6, comprising 4.6 % of cells,
219 is characterized by nucleosome organization, translation, and biosynthetic processes, with related
220 BP, MF, and CC tied to ribosomes, ribonucleoprotein complex and rRNA binding. Cluster 7,
221 representing 3 % of cells only, is characterized by multivesicular body sorting, vacuolar transport,

vacuole organization, and G protein-coupled receptor signaling, with related BP, MF, and CC of the ESCRT machinery.

Seven morphologically distinct immune cell types are identified by quantitative cytology and transcriptomic markers.

To better characterize the diversity of circulating hemocytes in *C. gigas*, cytological studies were performed using MCDH staining.

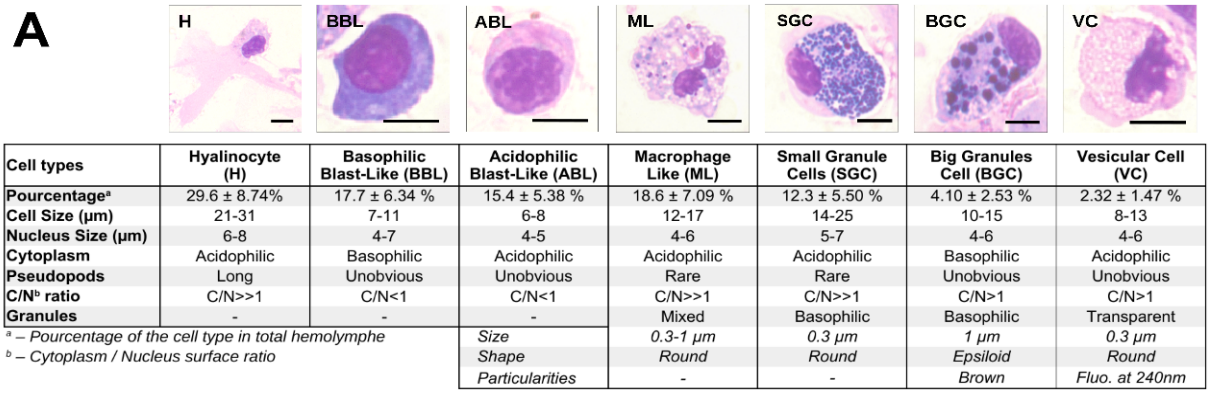

Cell types	Hyalinocyte (H)	Basophilic Blast-Like (BBL)	Acidophilic Blast-Like (ABL)	Macrophage Like (ML)	Small Granule Cells (SGC)	Big Granules Cell (BGC)	Vesicular Cell (VC)
Pourcentage[a]	29.6 ± 8.74%	17.7 ± 6.34 %	15.4 ± 5.38 %	18.6 ± 7.09 %	12.3 ± 5.50 %	4.10 ± 2.53 %	2.32 ± 1.47 %
Cell Size (µm)	21-31	7-11	6-8	12-17	14-25	10-15	8-13
Nucleus Size (µm)	6-8	4-7	4-5	4-6	5-7	4-6	4-6
Cytoplasm	Acidophilic	Basophilic	Acidophilic	Acidophilic	Acidophilic	Basophilic	Acidophilic
Pseudopods	Long	Unobvious	Unobvious	Rare	Rare	Unobvious	Unobvious
C/N[b] ratio	C/N>>1	C/N<1	C/N<1	C/N>>1	C/N>>1	C/N>1	C/N>1
Granules	-	-	-	Mixed	Basophilic	Basophilic	Transparent
Size				*0.3-1 µm*	*0.3 µm*	*1 µm*	*0.3 µm*
Shape				*Round*	*Round*	*Epsiloid*	*Round*
Particularities				-	-	*Brown*	*Fluo. at 240nm*

[a] – Pourcentage of the cell type in total hemolymphe
[b] – Cytoplasm / Nucleus surface ratio

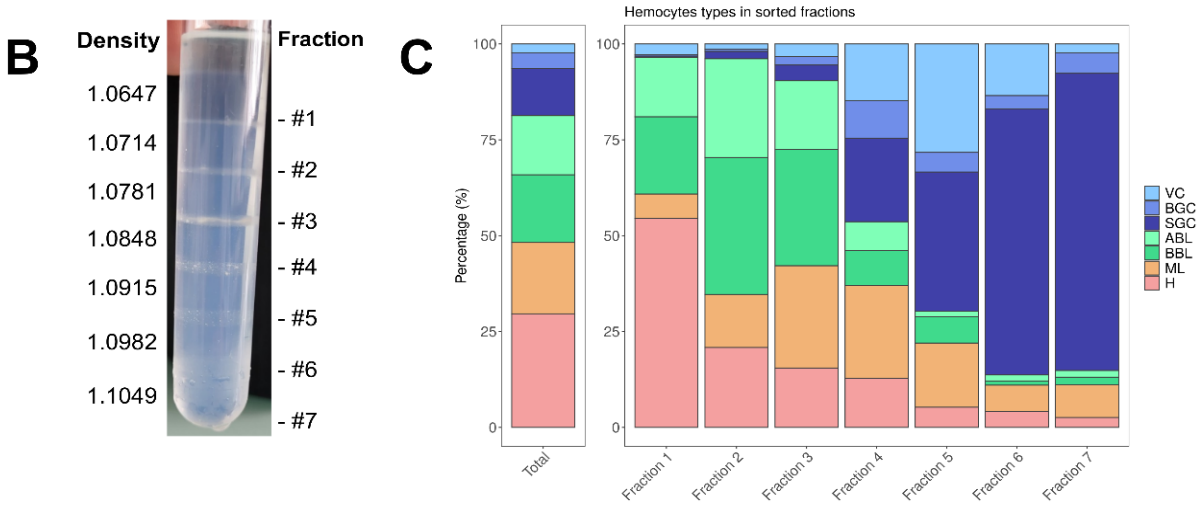

Fig 3. *C. gigas* naive hemocyte formula and Percoll gradient hemolymph fractionation (A) Morphology, percentages and characteristics of the 7 cell types identified by MCDH staining. **H** : Hyalinocyte, **ML** : Macrophage Like, **BBL** : Basophilic Blast Like cell, **ABL** : Acidophilic Blast Like cell, **SGC** : Small Granule Cell, **BGC** : Big Granule Cell, **VC** : Vesicular Cell. Scale bar : 5 µm. Hyalinocytes (54%) and blast cells (ABL & BBL) (35%) were predominant in the first fraction. The second fraction saw an increase in blasts (ABL 26%, BBL 36%) and a decrease in

hyalinocytes (21%). Fraction 3 had a mixed content with a decrease in hyalinocytes and blasts (15%), and majority being blasts and macrophage-like cells. Fraction 4 had an increase in granular cells (SGC 22%, BGC 10%, VC 15%) and a decrease in blasts (ABL 8%, BBL 9%). Fraction 5 showed an increase in small granule cells (36%) and vesicular cells (28%), and a decrease in big granule cells (5%). Fraction 6 had fewer hyalinocytes, macrophage-like, and blast cells compared to small granule cells and vesicular cells. The last fraction was mainly small granule cells (81%). **(B)** Hemocyte sorting on a discontinuous Percoll gradient. 7 fractions were identified along the gradient at the top of each density cushion (from d=1.0647 at #1 to d= 1.1049 at #7). **(C)** Representation of the average values (from 5 different fractionation experiments) of the different hemocyte types in the seven percoll gradient fractions compared to an average hemolymph composition of a naive oyster (Total). **VC** : Vesicular Cells, **BGC** : Big Granule Cells, **SGC** : Small Granule Cells, **ABL** : Acidophilic Blast Like cells, **BBL** : Basophilic Blast Like cells, **ML** : Macrophage Like cells and **H** : Hyalinocytes respectively. (**Supp. Fig. S4** for statistics).

We were able to define seven different hemocyte morphotypes : 3 non-granular (acidophilic blasts, basophilic blasts and hyalinocytes) and 4 granular (small granule cells, big granule cells, vesicular cells and macrophage-like) **(Fig. 3 and Supp. Fig. S3)**. Hyalinocytes (30% of total hemocytes) are large cells with an irregular spreading membrane, containing an azurophilic cytoplasm without granulations, the nucleus is irregular and varies in size (**Fig. 3A panel H**). Macrophage-like cells (19% of the hemocytes) present an irregular membrane punctuated by rare pseudopodia with a polylobed nucleus and a basophilic cytoplasm where polychromatic inclusions of various sizes could be observed (**Fig 3A. panel ML**). Basophilic blasts characterized by a basophil cytoplasm (**Fig. 3A panel BBL**) and acidophilic blasts with acidophil cytoplasm (**Fig. 3A panel ABL**) accounted for 18% and 15% of the total hemocytes respectively.

They are rounded cells without granulation with an uniform and regular dense nucleus and a high nucleo-cytoplasmic ratio. Small granule cells, (12% of the total hemocytes) have an irregular membrane punctuated by rare pseudopodia, an acidophilic cytoplasm, and numerous homogeneous purple granules (**Fig. 3A panel SGC**). Big granule cells (4% of the total hemocytes) are rounded cells with a basophilic cytoplasm containing large, slightly dark purple to black vesicles of heterogeneous size (**Fig. 3A panel BGC**). Vesicular cells representing 2% of the hemocytes, are rounded cells with acidophilic cytoplasm, rich in homogeneous transparent and fluorescent to UV light vesicles with an irregular nucleus (**Fig. 3A panel VC**). Only blasts (BBL, ABL) show a nucleo-cytoplasmic ratio less than 1, whereas the other hemocytes described show a nucleo-cytoplasmic ratio greater than 1.

To go further in the functional characterization of these diverse hemocyte morphotypes and to associate them with the transcriptomic clusters identified in the scRNA-seq, we improved a hemocyte fractionation approach using an isopycnic Percoll density gradient to sort the hemocytes (*29*). Cell sorting was performed using a discontinuous Percoll gradient with densities ranging from 1.0647 to 1.1049. Seven different density fractions were constituted (**Fig. 3B**) and hemocyte composition was then characterized by cytology visualization from each fraction (**Fig. 3A;** see also **Supp. Fig. S4** for statistical significance). Hemocyte morphotypes were unevenly distributed along the density gradient allowing a relative separation of the different cell populations (**Supp. Fig S4**). To summarize, hyalinocytes were significantly enriched in the first fraction, macrophage-like cells were significantly enriched in fraction 3 and in fraction 4. Acidophilic blasts were significantly enriched in fractions 2. Basophilic blasts were significantly enriched in fractions 2 and 3. Vesicular cells were enriched in fraction 5, big granule cells were enriched in the fraction 4 and small granule cells in fraction 6 and 7 (**Fig. 3C and Supp. Fig. S4**).

In order to identify the transcriptomic cell clusters corresponding to the different hemocyte morphotypes we used a RT-qPCR to detect the expression of different cluster-specific marker

genes in the different hemocytes in the Percoll density fractions. Marker genes were selected without a priori based only on their expression levels (Log2FC) and on their percentage of expression (Pct1 / Pct2 ratio) in the cluster of interest relative to all other cell clusters (**Table 2).** The expression level of each marker in the seven different clusters confirmed that the 14 selected marker genes were differentially expressed in each scRNA-seq transcriptomic cluster (**Supp. Fig. S5**).

Gene Number	Avg. Log2FC	Pct.1/Pct.2 Ratio	Cluster	Description	Marker Name
G8994	2.05	38.20	1	Laccase-24	LACC24
G8841	3.13	20.16		C-type lectin domain-containing protein	CLEC
G24846	2.31	31.52	2	EGF-like domain-containing protein 8	EGFL
G17277	3.21	23.00		Putative modulator of levamisole receptor-1	LEVAR
G22387	3.16	16.76	3	TGc domain-containing protein	TGC
G21091	5.51	7.69		X-box binding protein-like protein	XBOX
G35227	1.46	9.98	4	ML domain-containing protein	MLDP
G31074	0.94	6.51		High mobility group protein B1	HMGB1
G14441	3.35	11.01	5	Cubilin	CUBN
G12472	3.99	24.91		Galectin	GAL
G29512	3.20	246.25	6	Caveolin	CAV
G3767	6.45	41.11		Natterin-1	NAT1
G13140	3.12	40.00	7	DBH-like monooxygenase protein 1	MOX
G32859	3.90	23.82		G protein receptor F1-2 domain-containing protein	GPROT

Table 2. Table of the 14 marker genes specific to the different transcriptomic clusters. Gene number, average Log2FC, pct1/pct2 ratio (percentage of cells expressing this transcript in the cluster divided by the percentage of all other cells expressing this transcript) and cluster number are reported. The description is taken from our annotation and the marker name was derived from the description.

RT-qPCR expression profiles in the hemocyte fractions obtained from Percoll density gradient revealed distinct patterns according to the different transcriptomic cluster marker genes (**Fig. 4A**). Cluster 1 markers (LACC24 and CLEC) were overexpressed in fractions 1, 2, 3 and underexpressed in the other fractions relative to the total hemocytes. Cluster 2 markers (EGFL and LEVAR) showed a decreasing pattern of expression from fraction 1 to fraction 7. Cluster 3

markers (TGC and XBOX) showed significant increase in expression in fraction 4 to 7. Cluster 4 markers (MLDP and HMGB1) showed a gradually decreasing expression pattern from fraction 2 to fraction 7. Cluster 5 marker genes (GAL and CUBN) were underexpressed in fractions 4 to 7, but not differentially expressed in fractions 1 to 3 compared to total hemocytes. Cluster 6 marker genes (CAV and NAT1) were overexpressed in fraction 3, expressed similarly to total hemocytes in fraction 2, and underexpressed in fractions 1, and 4 to 7. Finally, cluster 7 marker genes (MOX and GPROT) were overexpressed only in fractions 3 to 7. A clear association between hemocyte morphotypes and 14 gene markers could be evidenced by correlation analysis and statistical validation (**Fig. 4B, Fig. 4C and Supp. Table S4**). Cluster 3 marker genes (TGC and XBOX) correlated positively (r = 0.74 & 0.75) and specifically with small granule cells (SGC). Cluster 7 markers (MOX and GPROT) specifically correlated (r = 0.68 and r = 0.56) with vesicular cells (VC). Cluster 2 markers (EGFL and LEVAR) correlated positively with hyalinocytes (H) (r=0.85 and r=0.81). We could not identify specific markers for blasts and macrophage-like cells.

A

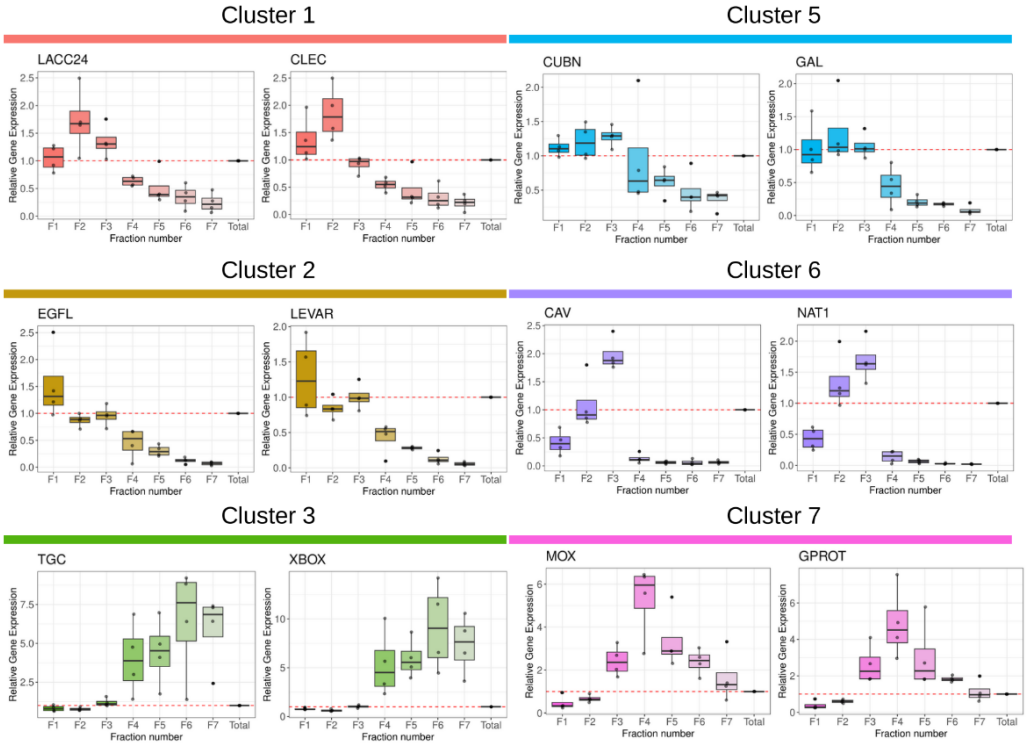

B

Hemocyte morphotypes

Percol fraction number	H	ML	BBL	ABL	SGC	BGC	VC
1	46.43	20.26	14.47	15.50	0.35	0.38	2.62
2	20.17	27.64	27.21	20.17	1.14	1.03	2.64
3	12.49	28.26	21.18	17.71	7.96	4.71	7.68
4	7.82	32.69	9.64	5.37	18.29	3.90	22.29
5	4.29	19.67	3.56	3.35	40.92	4.50	23.71
6	3.57	13.95	1.19	1.54	68.00	1.69	10.06
7	2.43	8.50	1.67	0.36	81.18	2.68	3.18

C

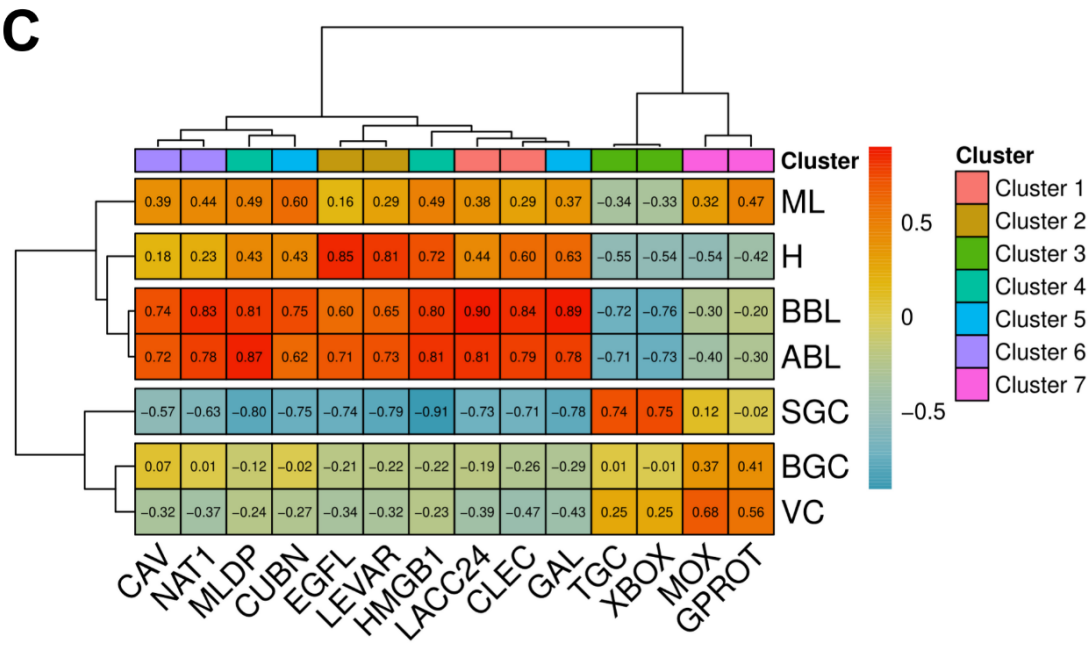

Fig 4. Characterization of the molecular markers specific to the different hemocyte morphotypes. (A) Relative expression level of the 14 markers in the different fractions after gradient density sorting. The graphs show the relative expression of genes compared to their expression in total hemocytes in the different fractions (red dotted line). Standard deviations were calculated on four independent experiments. **(B)** Average percentage of each hemocyte type in the 7 Percoll gradient fractions used to quantify marker gene expression by qPCR. **(C)** Correlation matrix between the relative gene expression of each marker gene in each fraction and the percentage of each hemocyte type in the same fractions. Values and color scale represent the Pearson correlation coefficient (r) ranging from -1 (inverse correlation) to +1 (full correlation). **H** : Hyalinocyte, **ML** : Macrophage Like, **BBL** : Basophilic Blast Like cell, **ABL** : Acidophilic Blast Like cell, **SGC** : Small Granule Cell, **BGC** : Big Granule Cell, **VC** : Vesicular Cell. **LACC24** : Laccase 24, **CLEC** : C-type lectin domain-containing protein, **EGFL** : EGF-like domain-containing protein 8, **LEVAR** : Putative regulator of levamisole receptor-1, **TGC** : TGc domain-containing protein, **XBOX** : X-box binding protein-like protein, **MLDP** : ML domain containing protein, **HMGB1** : High mobility group protein B1, **CUBN** : Cubilin, **GAL** : Galectin, **CAV** : Caveolin, **NAT1** : Natterin-1, **MOX** : DBH-like monooxygenase protein 1, **GPROT** : G protein receptor F1-2 domain-containing protein.

In conclusion, using RT-qPCR, cell sorting on Percoll gradients, and scRNA-seq analysis, we were able to accurately identify cell types corresponding to three transcriptomic clusters. Cluster 3 corresponds to small granule cells (SGC), cluster 2 to hyalinocytes (H), and cluster 7 to vesicular cells (VC). Cluster 3, cluster 2 and cluster 7 represent 17.8%, 23% and 3% of total cells analyzed by scRNA-seq, respectively. This is consistent with cytology data in which we counted 12.5% +/- 5% Small Granule Cells, 30 +/- 9.3% Hyalinocytes and 2.3 +/- 1.6% Vesicular Cells (**Fig. 1B and Fig. 3A**). Moreover molecular and cell functions deducted from GO-terms and

KEGG analyses (**Fig. 2**) were in agreement with the functions that could be expected to occur in these three cell types.

Only macrophage-like and small granule cells behave as professional phagocytes

In order to gain further insights into hemocytes functional specialization, hemocytes separated on the Percoll gradient were characterized functionally. Two hemocyte functions, namely phagocytosis and production of Reactive Oxygen Species (ROS), are known to carry out major cellular antimicrobial activities. Granular cells have been suggested to be the professional phagocytes specialized for these functions (*30*). Here, phagocytosis and oxidative burst were studied by using cell response toward zymosan particles (*31*).

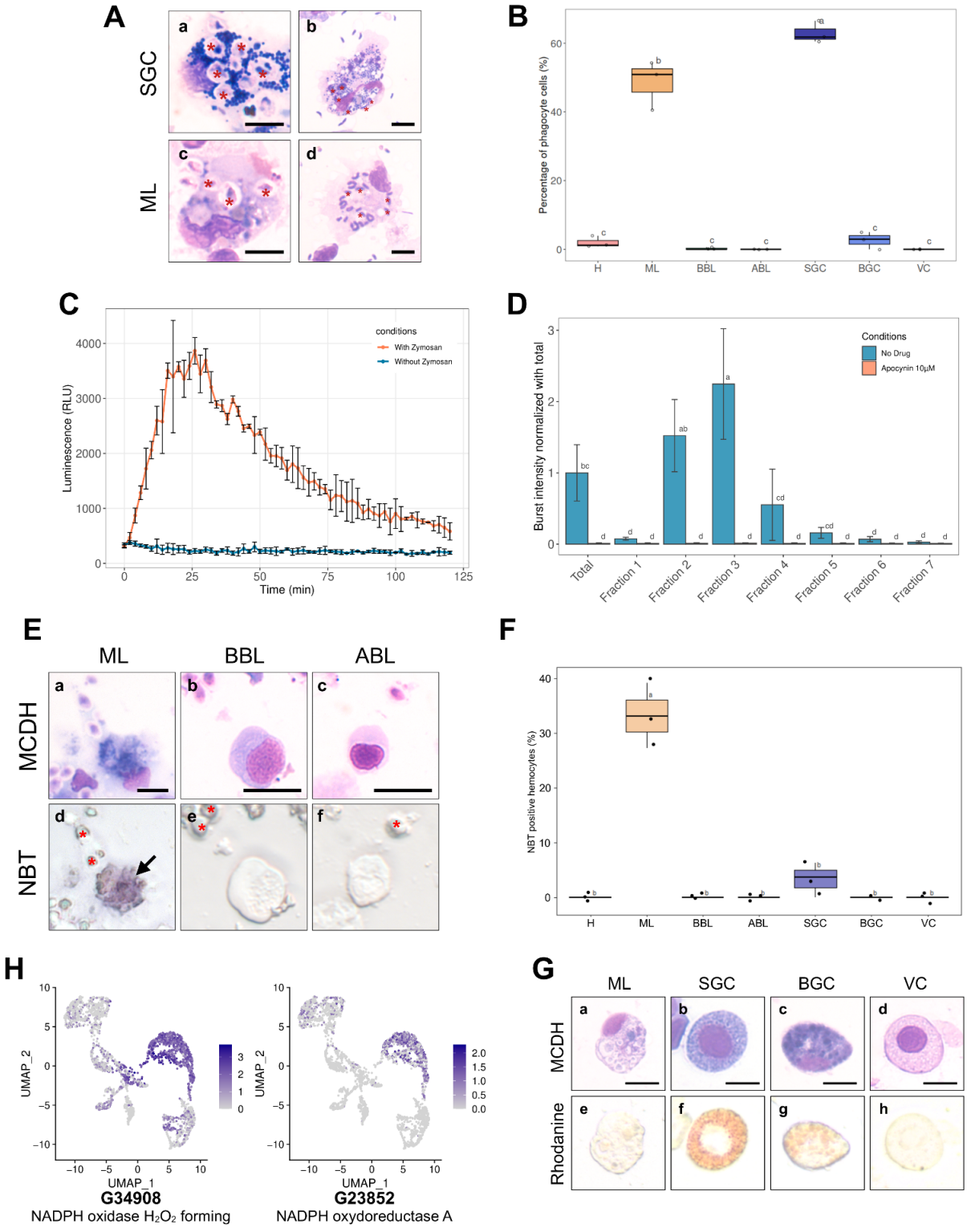

Fig 5. Phagocytosis, Reactive Oxygen Species production capacity and copper storage of hemocytes. (A) Images of small granule cells (**SGC**) and macrophage-like (**ML**) cells with phagocytosed zymosan particles (**panels a & c - red stars**) and *Vibrio tasmaniensis* LMG20012^T bacteria (**panels b & d - red stars**) from a total hemolymph sample. Scale bar : 5 µm. **(B)**

Quantification from 3 independent experiments of the phagocytic activity of each cell type for zymosan particles. Results of the quantification of the phagocytic activity of each cell type. The graph shows the result of 3 independent experiments. **(C)** Luminescence recording to detect the production of Reactive Oxygen Species (ROS). In orange, biphasic curve obtained on naive oyster hemolymph after zymosan addition at t = 0 min. In blue, the control condition corresponds to hemocytes without zymosan addition. **(D)** Graph showing the intensity of ROS production in each Percoll fraction. Normalized burst intensity was calculated from the luminescence peak obtained from each fraction. In blue, no drug was added to the experiment, in orange, ROS production was impaired by the addition of apocynin. **(E)** NBT (NitroBlueTetrazolium) staining of hemocytes exposed to zymosan particles. Hemocytes morphology after MCDH staining : Macrophage Like **(a**), Basophilic **(b)** and Acidophilic **(c)** Blast cells. NBT staining of the different hemocytes types **(d-f)**. Red stars show zymosan and bacteria particles. Black arrows identify Macrophage-Like cells. Scale bar : 10 µm **(F)** Quantification of NBT-positive cells present in the total hemolymph of oysters exposed to zymosan. **(H)** UMAP plots showing cells expressing NADPH oxidase found in the scRNA-seq dataset and their expression level. **(G)** Labeling of intracellular copper stores in *C.gigas* hemocytes. MCDH (upper panels) and rhodanine (lower panels) staining of oyster hemocytes to reveal copper accumulation. Scale bar : 10µm. For panels **(B)**, **(D)** and **(F)** The alphabetic characters displayed above the data points in each plot represent statistically significant differences among the groups, as determined by Tukey's test following ANOVA. Groups denoted by different letters differ significantly from each other at the $p < 0.05$ level of statistical significance. **H** : Hyalinocytes, **ABL** : Acidophilic Blast-Like cells, **BBL** : Basophilic Blast-Like cells, **ML** : Macrophage-Like cells, **SGC** : Small Granule Cells, **VC** : Vesicular Cells and **BGC** : Big Granule Cells.

The phagocytic activity of hemocytes was first tested on a sample of total oyster hemolymph. Cells were incubated with either zymosan particles or the bacterial strain *Vibrio tasmaniensis*

LMG20012^T for 1 hour. Only the small granule cells and the macrophage-like possess an efficient phagocytosis for both zymosan or vibrios, as observed after MCDH staining (**Fig. 5A, Supp. Fig. 6 and Supp. Fig. 7A**). Macrophage-like cells and small granule cells showed a phagocytosis activity of 49% and 55% respectively, and a phagocytosis index of 3.5 and 5.2 particles per cell respectively (**Fig. 5B and Supp. Fig. 7B**), as confirmed in 3 independent experiments. Very limited phagocytic activity was observed for hyalinocytes (1.7%), basophilic blasts (0.18%), and big granule cells (2.7%) with a phagocytosis index of 2, 1, and 2.5 particles per cell, respectively (**Fig. 5B and Supp. Fig. 7B**). These results confirmed that only small granule cells and macrophage-like cells behave as professional phagocytes harboring a strong phagocytosis activity.

Only macrophage-like cells produce Reactive Oxygen Species

We next examined the ability of *C. gigas* hemocytes in each Pecoll fraction to produce Reactive Oxygen Species (ROS) upon stimulation by zymosan using the Luminol oxidation assay. Luminol luminescence peaked 25 minutes after hemocyte (isolated from total hemolymph) were exposed to zymosan, which corresponds to a robust oxidative burst (**Fig. 5C**). The ROS production was dependent on a NADPH oxidase, as it was completely inhibited by the NADPH oxidase specific inhibitor apocynin (**Fig. 5C**). To identify which hemocyte types were involved in ROS production we tested Percoll density sorted hemocytes for oxidative burst activity. Fractions 2 and 3 displayed higher oxidative burst activity than the other fractions. The burst intensity of fraction 3 was twice that of total hemocytes, and fraction 2 also exhibited significantly increased burst activity. In contrast, fraction 4, showed a significant decrease in oxidative burst, and no activity was observed for fractions 1, 6 and 7 (**Fig. 5D**). These results indicate that NADPH-dependent oxidative burst activity is carried out by fractions enriched in macrophage-like (ML) cells and blast-like cells (ABL and BBL).

Previous studies have demonstrated that granular cells produce ROS (*30*). In contrast, we found that small granule cells collected in fraction 7 were incapable of producing ROS through an oxidative burst. To identify which type of hemocyte from blast-like cells and macrophage-like cells produce ROS within a few minutes after exposure to zymosan, ROS production was investigated using NitroBlueTetrazolium (NBT) reduction to directly stain hemocytes. This allows correlative microscopy using MCDH staining after the NBT reduction reaction. Macrophage-like cells were strongly and significantly stained by NBT reduction (33.2%) (**Fig. 5E, panels a & d**) while some small granule cells were lightly stained by NBT reduction (**Fig. 5F**). Blast-like cells, big granule cells, vesicular cells, and hyalinocytes were never NBT stained, confirming that these cell types were not involved in ROS production (**Supp. Fig. S7**). Altogether, these observations showed that small granule cells and macrophage-like cells are the two professional phagocytes among hemocytes but only macrophage-like cells are capable of oxidative burst upon exposure to zymosan. Based on these new functional data we further analyzed the expression level of NADPH-oxidase related enzymes in the scRNA-seq dataset. Cells of the cluster 1 were found to predominantly express two NADPH oxidase isoforms (gene numbers G34908 and G23852) compared to other clusters (**Fig. 5H**). Additionally, this cluster expresses macrophage-specific genes such as the angiopoietin receptor (**Table 1**), as well as maturation factors for dual oxidase, an enzyme involved in peroxide formation (**Supp. Fig. S8**). Collectively, these data indicated that cells of the transcriptomic cluster 1 corresponded to macrophage-like cells.

Small granule cells and big granule cells accumulate intracellular copper

The effect of copper on oyster hemocytes has long been studied due to its abundance in polluted marine areas (*21*). In addition, several studies have shown that *Vibrio* species pathogenic for *C. gigas* possess copper resistance genes, which are essential to survive inside hemocytes (*32*).

Therefore, we investigated which hemocyte types are involved in copper metabolism. To this end, total hemocytes isolated from naive oysters were stained with rhodanine to reveal copper storage in cells. Rhodanine staining revealed that 33 +/- 2 % of small granule cells and 30 +/- 10 % of big granule cells exhibited a specific reddish/brown staining indicative of high concentration of copper in their granules specifically (**Fig. 5G and Supp. Fig. S9**). These results provide the functional proof that SGC are specialized in metal homeostasis in addition to phagocytosis, as suggested by the scRNAseq data (Cluster 3).

Antimicrobial peptides are expressed by agranular cells, blasts and hyalinocytes

Antimicrobial peptides (AMPs) have long been studied for their role in invertebrate humoral immune response, and have been shown to be expressed by hemocytes including in *C. gigas* (*33*). We investigated whether different AMPs were expressed by different hemocyte cell types. Unfortunately, scRNA-seq analysis was not sensitive enough to reveal AMPs expression due to the limited sequencing depth, so we investigated AMPs expression by RT-qPCR on Percoll density fractionated hemocytes. Cg-Bigdefs 1-2, Cg-BPI and hemocyte defensin were found to be expressed mostly by agranular cells, blasts and hyalinocytes (ABL, BBL and H) (**Fig. 6A, B and C**). Among them, the expression of the four AMPs correlated with Blasts abundance whereas the expression of Cg-BigDefs 1-2 only correlated with hyalinocytes s (**Fig. 6D**). Granular cells (VC, ML, BGC and SGC) did not seem to express any of the AMPs that were analyzed here. These data suggest that some of the agranular cells are specialized in the production of humoral effectors.

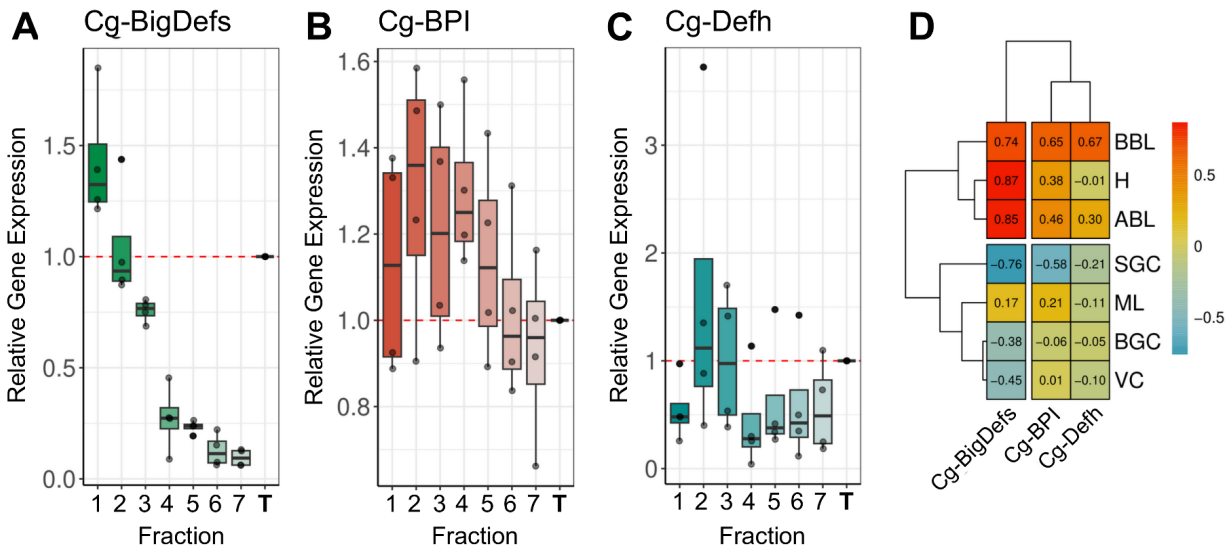

Fig 6. Hemocyte expression profiles of some antimicrobial peptides. (A) (B) and **(C)** Relative Gene Expression in the 7 Percoll hemocyte fractions of Big-Defensin1 & 2 (Cg-BigDefs), BPI (Cg-BPI) and hemocyte defensin (Cg-Defh) respectively compared to the gene expression level in unfractionated hemolymph. **(D)** Correlation matrix between the relative gene expression of BigDefensin1 & 2, BPI and hemocyte defensin gene in each fraction and the percentage of each hemocyte type in each fraction (**H** : Hyalinocytes, **ABL** : Acidophilic Blast Like, **BBL** : Basophilic Blast Like, **SGC** : Small Granule Cell, **ML** : Macrophage Like, **BGC** : Big Granule Cell, **VC** : Vesicular Cell. Values and color scale represent the Pearson correlation coefficient (r) ranging from -1 (inverse correlation) to +1 (full correlation).

Tentative model of hemocyte lineages and differentiation pathways in *C. gigas.*

Ontogeny, lineage and differentiation pathways are still mostly unknown in bivalves (*34*), but there are some clues for the presence of circulating and proliferating hemocytes progenitors in the hemolymph of *C. gigas* (*35*). GO-terms analysis of the 7 transcriptomic clusters revealed different functional signatures, among them the transcriptomic signature of the cluster 4 revealed a high expression level of ribosomal proteins (**Supp. Fig. S1J**), a particularity found in hematopoietic

stem cells in vertebrates (*36*) (*37*) (*38*). In addition, thanks to scRNAseq approaches, it is now possible to deduce differentiation pathways from mRNA splicing variant analysis using bioinformatic tools like Monocle3 (*39*). This revealed the overexpression of genes involved in the splicing, transcription and translation continuum in the same fourth cluster (**Fig. 2**) reinforcing the hypothesis of a pool of quiescent or immature cells capable of engaging in differentiation upon stimulation.

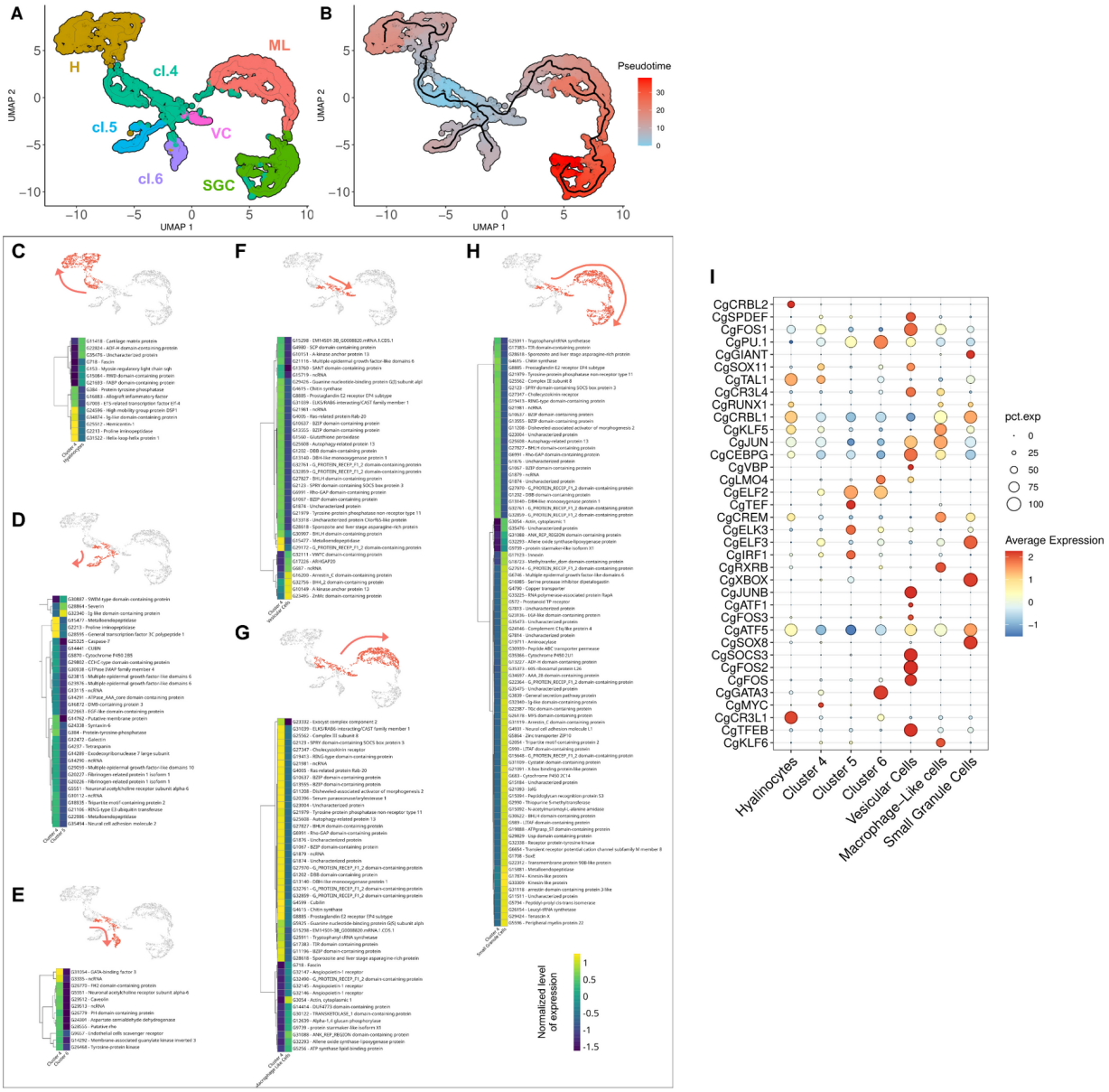

Figure 7. Pseudotime ordering of cells revealed 6 potential differentiation pathways of hemocytes. (A) UMAP plot of scRNA-seq analysis showing the 7 transcriptomic clusters used

for pseudotime analysis. 4 clusters were identified cytologically (SGC for small granule cells - cluster 3, H for hyalinocytes - cluster 2, ML for Macrophage Like - cluster 1 and VC for vesicular cells - cluster 7), cl.4, cl.5, and cl.6 represent clusters 4, 5, and 6, respectively. **(B)** Graphical representation (UMAP projection) of the Monocle 3 pseudo-time order of the clustered cells. Cluster 4 (cl.4) was used as the origin for the pseudotime analysis. **(C) (D) (E) (F) (G) and (H)** show gene expression level of selected marker genes obtained from the monocle3 trajectory analysis at the beginning and end of the modelized differentiation pathways (in red on the UMAP plot) from cluster 4 to hyalinocytes, to cluster 5 cells, to cluster 6 cells, to Vesicular Cells (VC), to Macrophage-Like cells (ML) and to Small Granule Cells (SGC) respectively. The color scale represents the normalized expression level of each gene. **(I)** Dot plot showing the average expression and the percentage of cells expressing identified transcripts encoding for transcription factors in the scRNA-seq dataset. Average expression is expressed in Log2FC.

Therefore, cluster 4 was chosen to enroot the pseudotime analysis to deduce differentiation pathways and cell lineages using Monocle3. (**Fig. 7A**). By temporally ordering the 2817 cells analyzed by scRNA-seq 5 cell lineages could be defined (**Fig. 7B**). Differentiation pathway 1 leads to hyalinocytes (H) (**Fig. 7C**). This transition is characterized by the downregulation of 8 genes, two of which are transcription factors (G7003 and G31522). The hyalinocyte cluster was also characterized by the overexpression of genes involved in cell contractility (G22824, G153 and G11418). Differentiation pathway 2 leads to cells of cluster 5 and are characterized by the downregulation of about 30 genes, and 3 genes related to Zn finger protein, actin cleavage and Ig-like domain proteins were specifically overexpressed (G30887, G28864 and G32340) (**Fig. 7D**). Differentiation pathway 3 leads to cells of cluster 6 and is characterized by the down-expression of 12 genes, and the upregulation of a GATA family transcription factor (G31054) (**Fig. 7E**). Pathways between cluster 4, 5 and 6 found by Monocle3 analysis were pseudo temporally short

and few specific markers were identified, suggesting that they were transcriptionally close. Differentiation pathway 4 leads to vesicular cells (VC) (**Fig. 7F**) where a large number of genes were silenced to give rise to these cells. Seven genes were specifically overexpressed in the VC (G32111, G17226, G687, G16200, G32756, G10149 and G23495). Interestingly, 6 genes encoding potential transcription factors were downregulated in this lineage (G30997, G10637, G1067, G13555, G2123 and G27827). Differentiation pathway 5 leads to macrophage-like cells (ML), and is characterized by the underexpression of 35 genes and the overexpression of 13 genes. Among the 35 genes, 6 of them were putative transcription factors (G2123, G10637, G13555, G27827, G1067 and G11196) (**Fig. 7G**). Finally, we can delineate a lineage ending in small granule cells (SGC) (**Fig. 7H**). This pathway involved cluster 4 (immature cells), VC, ML and SGC and was characterized by the downregulation of 27 genes, including 5 potential transcription factors (G10637, G13555, G27827, G1067 and G2123). SGC showed a distinct transcriptomic signature with 61 overexpressed genes, including 3 transcription factors (G1708, G21091 and G30622). Taken together, we propose that immature cluster 4 cells have pluripotent potential and can give rise to four terminally differentiated cell types which are cluster 5 and 6 cells, hyalinocytes and small granule cells and two other transient hemocyte cell types : vesicular cells and macrophage-like. All data from the Monocle3 analyses are available as Supplementary Data (**Supp. Fig. S10**).

Differentiation pathway analysis thus revealed the over- or under-expression of various transcription factors in the identified pathways. As transcription factors are well known master regulators of cell differentiation and can help to delineate cell lineages, we investigated combinatorial expression patterns of transcription factors among the different transcriptomic cell clusters. Based on GO-terms annotation we could isolate 28 different sequences corresponding to transcription factors from the scRNA-seq dataset. The transcription factor function was confirmed by manual annotation (**Supp. Table S5**) and **Figure 7I** shows the average expression profiles of

529 them in the different clusters and **Supplementary Figure S11** their expression levels in single
530 cells. Two transcription factors, CgATF5 and CgCRBL1 displayed a contrasting expression
531 profile with an increased average expression in macrophage-like cells, hyalinocytes and small
532 granule cells versus a low expression profile in cells in clusters 4, 5, 6 and vesicular cells. We also
533 identified transcription factors that were specifically expressed in the different transcriptomic
534 clusters : CgSPDEF, CgSOCS3, CgFOS and CgTFEB were specific for vesicular cells, CgSOX8,
535 CgXBOX and CgELF3 were specific for small granule cells, CgCR3L1 and CgTAL1 for
536 hyalinocytes, and CgJUN, CgKLF5, CgKLF6 and CgCREM for macrophage-like cells. Eight
537 other transcription factors were specifically identified in cluster 6 (CgGATA3, CgPU.1 and
538 CgELF2), cluster 5 (CgELF2, CgELK3 and CgIRF1) and cluster 4 (CgTAL1 and CgFOS1).
539 These data define potentially four distinct hematopoietic lineages originating from one type of
540 immature blast cells and give rise to hyalinocyte, SGC (via VC and ML), or two distinct
541 differentiated blast-like cells. We also identified a combination of transcription factors specific to
542 lineages and cell types that are potential master regulators of cell fate during hematopoiesis.

543 **Discussion**

544 The results of our study significantly improve the knowledge of *C. gigas* hemocyte functional
545 diversity and lineages. Using a combination of Single-cell RNA-seq and cytology, we identified
546 seven distinct hemocyte transcriptomic cell clusters, and the same number of morphotypes: four
547 granular cell types (big granule cells, macrophage-like cells, small granule cells and vesicular
548 cells), two distinct blast-like cells (basophilic and acidophilic blast-like cells), and one agranular
549 epithelial-like cell type (hyalinocytes). A major challenge was to find correlations between
550 transcriptomic and cytological data in order to fully define each distinct cytological cell type. This
551 challenge was overcome by combining multiple approaches using isopycnic Percoll density
552 gradient fractionation combined with expression of transcriptomic markers and functional assays
553 including phagocytosis, oxidative burst, copper accumulation, AMP expression and finally

pseudotime analysis of gene expression. All these results confirmed the historical classification of the 3 main cell groups : blasts, hyalinocytes and granular cells (*15*) and provided deeper insight into functional specificities of poorly characterized cell types. Particularly, we highlighted distinct transcriptional and functional subtypes among blasts and granular cells with complementary immune specialization and lineage relationships between cells.

One major result of the present study is the identification of cell types performing antimicrobial functions such as phagocytosis, accumulation of intracellular copper, an oxidative burst and antimicrobial peptide production, which have been extensively studied for their role in antibacterial and antiparasitic defenses as they are found in the large majority of invertebrates (*17*). However, the cell types specialized for these critical immune functions in bivalves, and in particular in oysters, have long been debated and the involvement of the different hemocyte subpopulations in immune functions has remained poorly understood.

Here, we uncover that the macrophage-like (ML) and the small granule cells (SGC) are the only hemocyte cell types that behave as professional phagocytes, as evidenced against Zymosan or *Vibrio*. These two distinct cell types could be distinguished functionally. First, we identified two distinct transcriptomic clusters for each cell type (Cluster 1 for ML / BGC and Cluster 3 for SGC). Second, only ML performed a measurable oxidative burst. Third, only SGC accumulated intracellular copper in specific granules. The two types of professional phagocytes belong to the same granular cell lineage, as determined by pseudotime analysis. The fact that ML could serve as a precursor for SGC could be counterintuitive. However, this is not an isolated case in invertebrate hemocytes. For instance, in *Drosophila* larvae (*40*), some populations of professional phagocytes, the sessile plasmatocytes, give rise to crystal cells or lamellocytes that are morphologically and functionally distinct from plasmatocytes (*41*). Like in the oyster, the

existence of multiple professional phagocytes is reminiscent of vertebrates macrophages, polynuclear neutrophils and dendritic cells, which harbor distinct functional specialization like efferocytosis (*42*), oxidative burst, NETosis, or antigen presentation (*43*).

The characterisation of professional phagocytes in oysters is of particular importance to better understand oyster-*Vibrio* interactions during pathogenesis. Some of the best studied oyster pathogens, including strains of *V. tasmaniensis* or *V. aestuarianus francensis* harbor virulence traits that allow them to interfere with phagocytic activity of hemocytes during pathogenesis as, for example, *V. tasmaniensis* that behaves as a facultative intracellular pathogen with phagocytosis-dependent cytotoxicity (*44*). Both *V. tasmaniensis* and *V. aestuarianus* also harbor resistance to copper toxicity through CopA and CusA/B transporters; this trait is essential for the survival and virulence in oyster (*45*), *32*). As we characterized here that SGCs are professional phagocytes with copper-rich granules, it is likely that the cellular interactions between SGCs and these vibrios is critical during antibacterial host response and pathogenesis. ML are phagocytes that harbor a very potent NADPH-oxidase dependent oxidative burst. Oxidative burst is recognized as a very rapid and potent antimicrobial response for professional phagocytes like Polynuclear neutrophils in mammals. Interestingly, NADPH dependent ETosis has been reported in *C. gigas i*n a similar manner than human neutrophils (*46*), this cell death is characterized by the projection of DNA extracellular traps that capture and kill some pathogens like *Vibrio* (*47*). Hence, it is tempting to speculate that ML could be also involved in ETosis.

The specialized functions harbored by the two other types of granular cells, the BGCs and the VCs, remain more elusive. A specific scRNAseq transcriptomic cluster for BGCs was difficult to identify, still, the level of expression of laccase 24 was found higher in a particular subcluster among ML (**Supp. Fig. S8**) and pseudo-time analysis highlighted the same subcluster as an

alternative differentiation state among ML (**Fig. 7B**). The enrichment of transcripts involved in oxido-reduction pathways, laccase 24 in particular, is in accordance with their potential role in melanisation and response to oxidative stress (*48*). Although melanin-like deposits have been observed in some cases of infestation by the parasites *Martelia* or B*onamia* in the Sydney rock oyster (*49*), this mechanism is not as strong as what is described in arthropods, which perform melanization through a prophenoloxidase activation cascade (*50*), (*51*). In many marine invertebrates (*48*), one type of hemocytes known as Brown Cells could relate to the BGCs that we describe here. In fact, when observed without any staining (as in **Fig. 5F**), their big granules with a yellow to dark brown content appears to correspond well with the historical description of brown cells that often infiltrate tissues (like gills) in animals exposed to polluted waters (*48*). These cells have thus been thought to be involved in detoxification processes. Based on our pseudotime analysis, we show that they likely derive from ML but with limited phagocytosis activity and rather specialized in melanisation and potentially heavy metal detoxification, as evidenced by rhodanine staining showing copper accumulation in some of their granules (**Fig. 5G**). To better understand the role of BGCs further studies should be performed either upon parasitic infestation or exposure to toxic stresses.

Finally, VC are granular cells that remain to be functionally characterized. They possess a strong intracellular vesicular trafficking and autophagy activity, as deduced from their transcriptomic profile. Still, we could not identify a particular immune-related function based on our functional assays. Their clear granules appear auto-fluorescent when illuminated with UV light (**Supp. Fig. S11**) but the biochemical nature of the content of these granules remains to be characterized. As they also appear as cell intermediate along the granular cell differentiation pathway in pseudotime analysis, they could represent functionally immature precursors of the other three granular cell types, like promyelocytes that possess specific azurophilic granules but are functionally immature precursors during granulocytes differentiation in human. However the enrichment of autophagy

related transcripts in VC calls for further investigation of a potential role in antiviral immunity as autophagy has been suggested to play a role in the response to OsHV-1 virus (*52*).

Hyalinocytes represent an homogenous cell type with only one morphotype matching one transcriptomic cluster. They originate from a specific and very different differentiation pathway than the granular cells, as deduced from pseudotime analysis. According to the literature, hyalinocytes are involved in the early stages of inflammation and can infiltrate wounds and interact with foreign particles. In the flat oyster *Ostrea edulis*, they contribute to shell production and wound healing (*53*). In the Sydney rock oyster they play a role in cell n aggregation (*54*), while in *C. virginica* (*55*) they contribute to encapsulation, which is reminiscent of lamellocytes in *Drosophila*. Our results indicate an important role in the immune response is their expression of antimicrobial peptides (AMPs). Indeed, *Cg*-BigDefs, which participates in the control of oyster microbiota (*56*), were found to be expressed both in hyalinocytes and blast-like cells. Supporting this immune function, hyalinocytes from the oyster *O. edulis* have been shown to express the AMP Myticin C (*57*). Among AMPs, we also identified that Cg-BPI and *Cg*-Defh, are more expressed in BBL, ABL than in other cell types. These results are somewhat unexpected as AMPs have often been considered to be stored in granules of granular cells but not in agranular cells (*16*). These results urge the need to reconsider a particular role for some agranular cell types in the active production of humoral immune effectors. Based on our findings, it can be hypothesized that hyalinocytes and/or the blast-like cells are a cellular target of the OsHV-1 virus, the causal agent of POMS, which dampens the expression of certain AMPs (*58*), thereby inducing a bacterial dysbiosis. Whether this is due to a decreased expression of AMPs and/or an inhibition of immature blast cells differentiation involved in the renewal of agranular cell types remains to be established.

One limit of our study is that we could not decipher the full complexity of blast-like cells, as we identified 3 clusters and only 2 morphotypes. Cell fractionation using Percoll gradient could not yield pure blast-enriched fractions (ABL and BBL), making precise functional characterization impossible. The enrichment in transcripts of the transcription synthesis degradation continuum aligns with the definition of undifferentiated blast-type cells and with the basophilic staining obtained in MCDH for BBL cells as immature blast cells are characterized by a basophilic cytoplasmic staining in human. However, our results show that some of these blast populations have the ability to produce AMPs, suggesting that these cells can also actively participate in the production of humoral effectors. Finally, whether these circulating immature cells are truly the stem cells at the origin of all hemocytes remains an open question.

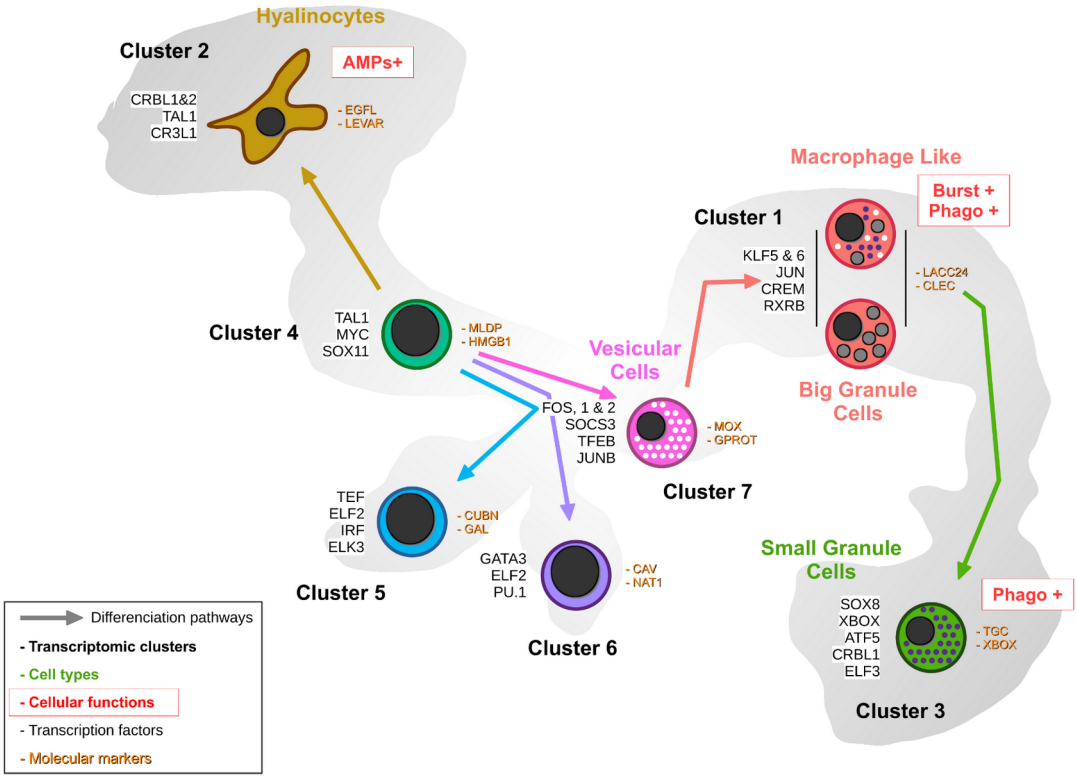

Figure 8. Proposed hemocyte ontology in *Crassostrea gigas* based on the transcriptomic, cytological and functional results obtained. Cells are shown colored according to the same

color code as the transcriptomic clusters. Cluster numbers and cell types are indicated. To the left of the cells are noted the overexpressed transcription factors and to the right the identified marker genes in each cluster. Functional characteristics of hyalinocytes, macrophage-like and small granule cells are marked in red.

In the animal kingdom, the innate immune system relies on specialized cells derived from pluripotent precursors through hematopoiesis. Transcription factors in particular have been found to be well conserved throughout the life kingdom from invertebrates to vertebrates. However in bivalves, the mechanisms underlying their functional differentiation are only partially available or understood (*59*). Recent researches have suggested the existence of potential hemocyte progenitors, also known as blast-like cells in several bivalve species, including clams, mussels, scallops, marine mussels, freshwater mussels, oysters, pearl oysters, and wing shells (*59*), however different models for hematopoiesis in bivalve have been proposed and long been debated without a clear consensus and definitive proofs. Thanks to single-cell RNA sequencing and pseudotime analysis, we can now propose a refined model of hematopoiesis at an unprecedented level of detail. In this model, the different types of hemocytes are likely produced through four differentiation pathways originating from a common progenitor. One pathway leads to the formation of agranular hyalinocytes, while another independent pathway gives rise to the granular cells, including VC, ML, BGC, and SGC. Additionally, there are two other differentiation pathways that potentially lead to terminally differentiated blast-like cells. The differentiation of mature hemocytes involves the establishment of lineage-specific gene expression profiles that rely on transcription factors to modulate the expression of their target genes. Here, we identified combination of transcription factor that are differentially expressed during *C. gigas* hematopoiesis and are specific of differentiation stages and cell lineages, among them many well-known

hematopoietic transcription factors like GATA, PU-1, TAL1 and SOX factors are positioned in this model of *C. gigas* hematopoiesis (*60*), (*61*), (*62*) (**Fig. 8**).

Our study significantly advances our understanding of bivalve immunity, particularly in comparison to arthropods. By introducing a standardized reference hemocytogram for oysters using MCDH staining, defining cell type specific markers, and key transcription factors likely involved in cell fate determination, and clarifying the functions of different hemocytes, we set the ground for future in depth studies. This will allow further studies of the oyster's immune response to various biotic and abiotic stress at the cellular level. A better comprehension of antiviral and antibacterial responses in bivalves and improving our understanding of immune priming and immune memory at the cellular level in bivalves will improve health and population management for sustainable aquaculture production. Moreover, they will contribute to the broader field of evolutionary immunology by enabling comparative studies and deciphering the diversification of immune cells and immunity related genes in a protostome.

Materials and Methods

Conservation of oysters

The work described here was performed using two different sources of oysters of the same species *Crassostrea (Magallana) gigas*. ISA (Ifremer Standardized Oysters - La tremblade - France) oysters for the scRNA-seq experiment and oysters provided by a local supplier (https://www.huitres-bouzigues.com). Animals were washed and kept in 10 L tanks containing seawater and a bubbler to oxygenate and homogenize the water. Water was changed daily and oyster health was monitored. All animals used in this study were 18 months of age.

Hemocyte collection and processing

Crassostrea gigas hemocytes were obtained by puncture of the adductor muscle from live animals. The oyster shell was incised with forceps on the posterior side. Hemolymph was

collected using a 23Gx1" needle mounted on a 5 mL syringe prefilled with 2 mL of ice-cold Alsever modified medium (20.8 g glucose – 8 g trisodium citrate - 22.5 g sodium chloride - 0.4 g BSA - pH=7.5). Samples were centrifuged for 4 minutes at 200 g – 4 °C and the supernatant was removed and replaced with 1 mL of fresh Alsever modified medium. Each hemocyte sample was thoroughly checked for quality, counted under a microscope using KOVA (Kova International, USA) slides, and stored on ice prior to processing. For scRNA-seq analysis, resuspended hemocytes were filtered on 30 µm filters, counted, the solution was adjusted to 1.10^6 cells per mL and stored on ice prior to 10X genomic library preparation.

C. gigas genome annotation

The *C. gigas* genome (Genbank GCA_905397895.1) (*27*) was used as a reference. Prior to annotation, the longest CDS sequences were extracted from the gff3 file. Annotation was realized using the ORSON script (https://gitlab.ifremer.fr/bioinfo/workflows/orson). ORSON combines state-of-the-art tools for annotation processes within a Nextflow pipeline. ORSON script performs sequence similarity search with BLAST (*63*) against Uniprot-Swissprot and Uniprot-trEMBL database, and functional prediction with InterProScan (*64*) and eggNOG (*65*) orthogroup annotation. Interproscan analysis was performed against Pfam, Prosite, CDD, TIGR, SMART, SuperFamily, PRINTS and Hamap databases. Results were collected and processed using Blast2GO (*66*) for annotation mapping and validation.

Drop Seq based scRNA-seq library generation

The 10X Genomics protocol, Single Cell 3' Reagent Kits v2 User Guide from the manufacturer (10X Genomics, USA) was followed to prepare gel in emulsion beads (GEM) containing single cells, hydrogel beads, and reverse transcription reagents, perform barcoded cDNA synthesis, and generate sequencing libraries from pooled cDNAs. The concentration of single cell suspensions was approximately 1000 cells / µL, as estimated by manual counting, and cells were loaded according to the 10X protocol to capture approximately 3000 cells per reaction. Library

construction (after GEM digestion) was performed using 10X reagents according to the manufacturer. Libraries (paired end reads 75 bp) were sequenced on an Illumina NovaSeq (Illumina, USA) using two sequencing lanes per sample.

scRNA-seq analysis

Reads were aligned to the *C. gigas* reference genome (Genbank GCA_905397895.1) (*27*) using STAR solo software (v 2.7.10) (*23*). Unique molecular identifiers (UMIs) were extracted and counted for each cell, and an expression matrix was generated for further analysis. Single-cell RNA sequencing (scRNA-seq) data analysis was performed using the R programming language (version 4.2.1) (R Core Team, 2018) and the Seurat package (version 4.3.0) (*67*). The data were then pre-processed to remove unwanted sources of variation and to normalize gene expression. Cells with small library sizes and a high proportion of mitochondrial genes were excluded. Data normalization was performed using the SCTransform method. After normalization, highly variable genes were identified using the FindVariableFeatures function and the top variable genes were selected for downstream analyses. Dimensionality reduction was performed using Principal Component Analysis (PCA), subsequently, uniform manifold approximation and projection (UMAP) was applied to visualize the data. Cell clustering was performed using the 'FindClusters' function, using the previously identified significant principal components (dims = 6) and a resolution parameter (r = 0.1) to define cluster granularity. Differential expression analysis was performed using the 'FindAllMarkers' (pct.min = 0.25) function to identify genes differentially expressed between clusters, with statistical significance determined using the Wilcoxon rank sum test. Functional enrichment analysis of differentially expressed genes was performed using gene set enrichment analysis (RBGOA) (*68*).

KEGG pathway analysis

KEGG analysis was performed using DAVID Bioinformatics Resources (NIAID/NIH) (*26*). Gene lists of specifically overexpressed genes in each cluster were obtained after scRNA-seq

processing (genes with Log2FC > 0.25 and significant p-value < 0.001) and used for KEGG annotation. The *C. gigas* reference genome from the DAVID bioinformatics resource was used for this analysis, with thresholds of 2 for counts and 0.05 for EASE value (p-value). KEGG annotation results were post-processed and presented as a heatmap showing KEGG pathway, fold enrichment, p-value significance and number of positive terms.

Rank Based Gene Ontology Analysis

RBGOA first clusters GOs according to their representative genes to identify the most significant GOs, and then ranks the identified biological processes according to their average expression levels (over all representative genes). Finally, biological processes, molecular functions and cellular components significantly enriched in DEGs are identified by a Mann-Whitney rank test with a strict FDR correction. The files generated by the GO-MWU scripts (https://github.com/z0on/GO_MWU) were post-processed to extract the category names and the fraction indicating the number of "good candidates" relative to the total number of genes belonging to that category. The "good candidates" were the genes that exceed an arbitrary 'absValue' cutoff (defined as 0.001) in their significance measure. The results were presented as a heatmap.

Percoll Density Gradient Separation of Hemocytes

A concentration series of Percoll (Cytiva, Sweden) diluted in Alsever modified medium was prepared as follows: 10, 20, 30, 40, 50, 60 and 70 % (vol/vol). Discontinuous density gradients (from 10 % Percoll with a density of 1.0647 to 70 % Percoll with d=1.1049) were made using 1.5 mL of each concentration and loaded with 1 mL of the hemocyte suspension corresponding to approximately 2.10^7 cells. Centrifugation was performed (30 min, 800 g, 4 °C) in a swinging bucket on a Beckman Coulter JS-13.1 rotor (Beckman Coulter, USA). Hemocytes concentrated at each density interface were collected separately with a 70 mm long 20Gx2.75" needle mounted on a 1 mL syringe. The hemocytes were then washed from the Percoll by adding 10 mL of ice-

cold Alsever modified medium, pelleted by centrifugation (10 min, 200 g, 4°C) and resuspended in Alsever modified medium or filtered sea water.

Cytological description of the hemocyte populations

200,000 fresh hemocytes were seeded onto a slide using a Cytospin 4 centrifuge (Thermo Scientific, USA). The samples were then stained using the panoptic MCDH (Micro Chromatic Detection for Hematology) (Cellavision, Sweden) staining protocol. This protocol produces purple hues typical of Romanowsky-Giemsa staining results. After staining, the samples were observed using a LEICA DMR (Leica AG, Germany) transmitted light microscope with a 40x magnification objective. Each slide was imaged and the hemocytes were counted and characterized based on their morphology.

Real Time-quantitative Polymerase Chain Reaction (RT-qPCR)

Total RNA was extracted using the RNeasy kit (Qiagen, the Netherlands) and cDNA was synthesized from 1 µg total RNA using the Superscript IV kit (ThermoFisher Scientific, USA) with oligo(dT) primers. RT-PCR was performed on LightCycler© 480 thermocycler using the SYBR Green 1 Master kit (Roche, Switzerland). Primers were used at 200 nM. Primer sequences are listed in **Supplementary Table S3**. Expression was normalized to *Cg-rps6* reference gene. The standard cycling conditions were 95°C pre-incubation for 3 minutes followed by 40 cycles of 95°C for 10 seconds, 60°C for 20 seconds, and 72°C for 25 seconds. Each pair of primers was first tested and validated on a total hemocyte RNA preparation to control melting curves and establish calibration lines.

Oxidative Burst Assay

The production of reactive oxygen species was quantified by luminescence assay. Briefly, hemocytes from hemolymph puncture or Percoll density gradient were washed once with filtered sterile water. 50 µL of hemocytes were plated in triplicate on a 96-well plate (3.10^5 cells/cm²). 50 µL of 40 mM luminol (Merck and Co, USA) was added to each well. After 45 minutes of

incubation at room temperature, the oxidative burst was induced by adding 100 µL of zymosan (Merck and Co, USA) at a multiplicity of infection (MOI) of 50:1. The plate was immediately placed in a luminescence microplate reader Berthold Centro XS3 LB 960 (Berthold GmbH, Germany) to measure luminescence emission every 2 minutes for 2 hours.

Phagocytosis assay

400 µL of filtered, sterile water-washed hemocytes were seeded in a 24-well plate at a concentration of 3.10^5 cells/cm². After 15 minutes, 50 µL of zymosan was added to the fractions at a MOI of 20:1. For LMG20012t Vibrio, 50 µL of bacteria was added to a total hemolymph at a MOI of 5:1. After 1 hour of contact at room temperature, the cells were resuspended and 200 µL of the suspension was applied to a microscope slide using a Cytospin centrifuge. The slides were then stained with MCDH and observed under a transmitted light microscope LEICA DMR with 40x magnification objective (Leica AG, Germany) to count phagocytic cells.

NitroBlueTetrazolium (NBT) staining

The production of reactive oxygen species was measured using NitroBlue Tetrazolium reduction after zymosan stimulation. Briefly, 1 mL (1.10^6 cells) of hemocyte solution was mixed with 50 µL of filtered NBT solution (15 mg/mL in water). Zymosan was added at a 4:1 MOI and the mixture was incubated at room temperature for 10 minutes on a rocking shaker, then 50 µL of each sample was plated onto glass coverslips and observed under a transmitted light microscope LEICA DMR with 40x magnification objective (Leica AG, Germany) to count NBT-positive cells. The positions of positive NBT cells were recorded prior to MCDH staining to identify hemocyte types.

Rhodanine copper staining of hemocytes

The storage of copper by hemocytes was examined by Rhodanine staining. Briefly, 1.10^5 hemocytes were plated on Superfrost slides using a cytospin and circled with a hydrophobic pen to retain the staining solution. The Copper Stain Kit (SkyTek, USA) was used to stain the

hemocytes. As described by the kit manufacturer, one drop of Rhodanine solution was added to 9 drops of acetate to form the working solution. Five drops were placed on the cytospin cells and a 5 mL Eppendorf tube with the cap removed was placed over the cells to prevent evaporation of the working solution. The slide and the balanced Eppendorf tube were placed on a beaker of boiling distilled water for 20 minutes. The slide was then washed with 5 drops of acetate and 3 drops of hematoxylin were placed on the slide for 1 minute at room temperature. The slides were then washed a final time with acetate and observed under a LEICA DMR transmitted light microscope with a 40x magnification objective (Leica AG, Germany) to count rhodanine-positive cells. The positions of rhodanine-positive cells were recorded prior to MCDH staining to identify hemocyte types.

Pseudotemporal ordering of cells with Monocle3

Cells from the *C. gigas* dataset were analyzed using Monocle3 (https://github.com/cole-trapnell-lab/monocle3) (*39*). The Monocle3 analysis was performed on the Seurat object after processing described above. Clustering information (features, genes, partitions, clusters and UMAP coordinates) was transferred to a CDS object. The cell trajectory was calculated using the *learn_graph* function. Three lineages were selected by using *choose_graph_segments* function. The gene expression along pseudotime data was extracted from the result. Then the data were used to plot genes along pseudotime in three lineages using ggplot2 v3.4.4 R package and the heatmap was generated using pheatmap v1.0.12 R package.

Statistical Analysis

To assess differences between samples, statistical analysis was performed using (version 4.2.1) (R Core Team, 2018) and appropriate packages. All data were examined for normality, and statistical tests were chosen accordingly. For normally distributed data, one-way analysis of variance (ANOVA) was used. For cytological analysis, 7 different hemolymph samples were used. Oysters were provided by our local supplier) and approximately 300 hemocytes were counted per sample.

For Percoll density gradient separation, 7 independent experiments were performed. A Tukey test was used to evaluate the statistical difference between the proportions of hemocyte types. The phagocytic capacity of hemocytes was tested in three independent experiments and statistical differences were evaluated using the Tukey test for both the phagocytic capacity between hemocyte types and the number of particles per phagocyte. Finally, oxidative burst capacity was tested 3 times on Percoll-separated hemocytes. The Tukey test was also used to assess statistical differences between conditions. The null hypothesis was rejected at a significance level of $p = 0.05$.

References

1. Y. M. Bar-On, R. Phillips, R. Milo, The biomass distribution on Earth. *Proc. Natl. Acad. Sci.* **115**, 6506–6511 (2018).
2. B. Leicester Bayne, *Biology of Oysters* (Academic Press, 1st Edition., 2017)vol. 41.
3. G. Zhang, L. Li, J. Meng, H. Qi, T. Qu, F. Xu, L. Zhang, Molecular Basis for Adaptation of Oysters to Stressful Marine Intertidal Environments. *Annu. Rev. Anim. Biosci.* **4**, 357–381 (2016).
4. FAO, Global aquaculture production. Fisheries and aquaculture division (2023).
5. F. Pernet, C. Lupo, C. Bacher, R. J. Whittington, Infectious diseases in oyster aquaculture require a new integrated approach. *Philos. Trans. R. Soc. B Biol. Sci.* **371**, 20150213 (2016).
6. A. Alfjorden, M. Areskog, D. Bruno, R. Carnegie, D. Cheslett, S. Feist, S. Ford, S. Jones, A. Lillehaug, L. Madsen, T. Renault, N. Ruane, P. Vennerstrom, New Trends in Important Diseases Affecting the Culture of Fish and Molluscs in the ICES Area 2002– 2015. *ICES Coop. Res. Rep.*, doi: 10.17895/ices.pub.2800 (2017).
7. J. de Lorgeril, A. Lucasson, B. Petton, E. Toulza, C. Montagnani, C. Clerissi, J. Vidal-Dupiol, C. Chaparro, R. Galinier, J.-M. Escoubas, P. Haffner, L. Dégremont, G. M. Charrière, M. Lafont, A. Delort, A. Vergnes, M. Chiarello, N. Faury, T. Rubio, M. A. Leroy, A. Pérignon, D. Régler, B. Morga, M. Alunno-Bruscia, P. Boudry, F. Le Roux, D. Destoumieux-Garzón, Y. Gueguen, G. Mitta, Immune-suppression by OsHV-1 viral infection causes fatal bacteraemia in Pacific oysters. *Nat. Commun.* **9**, 4215 (2018).
8. N. M. Coyle, C. O'Toole, J. C. L. Thomas, D. Ryder, E. J. Feil, M. Geary, T. P. Bean, A. W. Joseph, A. Waine, D. Cheslett, D. W. Verner-Jeffreys, Vibrio aestuarianus Clade A and Clade B isolates are associated with Pacific oyster (Crassostrea gigas) disease outbreaks across Ireland. bioRxiv [Preprint] (2023). https://doi.org/10.1101/2023.04.06.535062.
9. A. Mesnil, M. Jacquot, C. Garcia, D. Tourbiez, L. Canier, A. Bidois, L. Dégremont, D. Cheslett, M. Geary, A. Vetri, A. Roque, D. Furones, A. Garden, P. Orozova, I. Arzul, M. Sicard, G. M. Charrière, D. Destoumieux-Garzón, M.-A. Travers, Emergence and clonal expansion of Vibrio aestuarianus lineages pathogenic for oysters in Europe. *Mol. Ecol.* **32**, 2869–2883 (2023).
10. D. Oyanedel, A. Lagorce, M. Bruto, P. Haffner, A. Morot, Y. Labreuche, Y. Dorant, S. de La Forest Divonne, F. Delavat, N. Inguimbert, C. Montagnani, B. Morga, E. Toulza, C. Chaparro, J.-M. Escoubas, Y. Gueguen, J. Vidal-Dupiol, J. de Lorgeril, B. Petton, L. Degremont, D. Tourbiez, L.-L. Pimparé, M. Leroy, O. Romatif, J. Pouzadoux, G. Mitta, F. Le Roux, G. M. Charrière, M.-A. Travers, D. Destoumieux-Garzón, Cooperation and cheating orchestrate Vibrio assemblages and polymicrobial synergy in oysters infected with OsHV-1 virus. *Proc. Natl. Acad. Sci.* **120**, e2305195120 (2023).
11. T. Rubio, D. Oyanedel, Y. Labreuche, E. Toulza, X. Luo, M. Bruto, C. Chaparro, M. Torres, J. de Lorgeril, P. Haffner, J. Vidal-Dupiol, A. Lagorce, B. Petton, G. Mitta, A. Jacq, F. Le Roux, G. M. Charrière, D. Destoumieux-Garzón, Species-specific mechanisms of cytotoxicity toward immune cells determine the successful outcome of Vibrio infections. *Proc. Natl. Acad. Sci.* **116**, 14238–14247 (2019).
12. Y. Labreuche, F. Le Roux, J. Henry, C. Zatylny, A. Huvet, C. Lambert, P. Soudant, D. Mazel, J.-L. Nicolas, Vibrio aestuarianus zinc metalloprotease causes lethality in the Pacific oyster Crassostrea gigas and impairs the host cellular immune defenses. *Fish Shellfish Immunol.* **29**, 753–758 (2010).
13. M. Lafont, A. Vergnes, J. Vidal-Dupiol, J. de Lorgeril, Y. Gueguen, P. Haffner, B. Petton, C. Chaparro, C. Barrachina, D. Destoumieux-Garzon, G. Mitta, B. Gourbal, C. Montagnani, A Sustained Immune Response

Supports Long-Term Antiviral Immune Priming in the Pacific Oyster, Crassostrea gigas. *mBio* **11**, 10.1128/mbio.02777-19 (2020).
14. M. Fallet, C. Montagnani, B. Petton, L. Dantan, J. de Lorgeril, S. Comarmond, C. Chaparro, E. Toulza, S. Boitard, J.-M. Escoubas, A. Vergnes, J. Le Grand, I. Bulla, Y. Gueguen, J. Vidal-Dupiol, C. Grunau, G. Mitta, C. Cosseau, Early life microbial exposures shape the Crassostrea gigas immune system for lifelong and intergenerational disease protection. *Microbiome* **10**, 85 (2022).
15. N. R. de la Ballina, F. Maresca, A. Cao, A. Villalba, Bivalve Haemocyte Subpopulations: A Review. *Front. Immunol.* **13** (2022).
16. E. Bachère, R. D. Rosa, P. Schmitt, A. C. Poirier, N. Merou, G. M. Charrière, D. Destoumieux-Garzón, The new insights into the oyster antimicrobial defense: Cellular, molecular and genetic view. *Fish Shellfish Immunol.* **46**, 50–64 (2015).
17. J.-M. Escoubas, B. Gourbal, D. Duval, T. J. Green, G. M. Charrière, D. Destoumieux-Garzón, C. Montagnani, "Immunity in Molluscs" in *Encyclopedia of Immunobiology*, M. J. H. Ratcliffe, Ed. (Academic Press, Oxford, 2016; https://www.sciencedirect.com/science/article/pii/B9780123742797120041), pp. 417–436.
18. A. S. Mount, A. P. Wheeler, R. P. Paradkar, D. Snider, Hemocyte-Mediated Shell Mineralization in the Eastern Oyster. *Science*, doi: 10.1126/science.1090506 (2004).
19. W. S. FısıER, "Environmental influence on bivalve hemocyte function" in *Am Fish Soc Symp* (1988; https://www.researchgate.net/profile/William-Fisher-29/publication/285361443_Environmental_influence_on_bivalve_hemocyte_function/links/5d435d5f299bf1995b5e5d4c/Environmental-influence-on-bivalve-hemocyte-function.pdf)vol. 18, pp. 225–237.
20. T. V. Nguyen, A. C. Alfaro, F. Merien, Omics approaches to investigate host–pathogen interactions in mass mortality outbreaks of Crassostrea gigas. *Rev. Aquac.* **11**, 1308–1324 (2019).
21. J. Meng, G. Zhang, W.-X. Wang, Functional heterogeneity of immune defenses in molluscan oysters Crassostrea hongkongensis revealed by high-throughput single-cell transcriptome. *Fish Shellfish Immunol.* **120**, 202–213 (2022).
22. R. D. Rosa, P. Alonso, A. Santini, A. Vergnes, E. Bachère, High polymorphism in big defensin gene expression reveals presence–absence gene variability (PAV) in the oyster Crassostrea gigas. *Dev. Comp. Immunol.* **49**, 231–238 (2015).
23. B. Kaminow, D. Yunusov, A. Dobin, STARsolo: accurate, fast and versatile mapping/quantification of single-cell and single-nucleus RNA-seq data. bioRxiv [Preprint] (2021). https://doi.org/10.1101/2021.05.05.442755.
24. C. Peñaloza, A. P. Gutierrez, L. Eöry, S. Wang, X. Guo, A. L. Archibald, T. P. Bean, R. D. Houston, A chromosome-level genome assembly for the Pacific oyster Crassostrea gigas. *GigaScience* **10**, giab020 (2021).
25. R. Satija, J. A. Farrell, D. Gennert, A. F. Schier, A. Regev, Spatial reconstruction of single-cell gene expression data. *Nat. Biotechnol.* **33**, 495–502 (2015).
26. B. T. Sherman, M. Hao, J. Qiu, X. Jiao, M. W. Baseler, H. C. Lane, T. Imamichi, W. Chang, DAVID: a web server for functional enrichment analysis and functional annotation of gene lists (2021 update). *Nucleic Acids Res.* **50**, W216–W221 (2022).
27. C. Peñaloza, A. P. Gutierrez, L. Eöry, S. Wang, X. Guo, A. L. Archibald, T. P. Bean, R. D. Houston, A chromosome-level genome assembly for the Pacific oyster Crassostrea gigas. *GigaScience* **10**, giab020 (2021).
28. R. M. Wright, G. V. Aglyamova, E. Meyer, M. V. Matz, Gene expression associated with white syndromes in a reef building coral, Acropora hyacinthus. *BMC Genomics* **16**, 371 (2015).
29. E. Bachère, D. Chagot, H. Grizel, Separation of Crassostrea gigas hemocytes by density gradient centrifugation and counterflow centrifugal elutriation. *Dev. Comp. Immunol.* **12**, 549–559 (1988).
30. W. Wang, M. Li, L. Wang, H. Chen, Z. Liu, Z. Jia, L. Qiu, L. Song, The granulocytes are the main immunocompetent hemocytes in Crassostrea gigas. *Dev. Comp. Immunol.* **67**, 221–228 (2017).
31. C. Lambert, P. Soudant, G. Choquet, C. Paillard, Measurement of Crassostrea gigas hemocyte oxidative metabolism by flow cytometry and the inhibiting capacity of pathogenic vibrios. *Fish Shellfish Immunol.* **15**, 225–240 (2003).
32. A. Mesnil, M. Jacquot, C. Garcia, D. Tourbiez, L. Canier, A. Bidois, L. Dégremont, D. Cheslett, M. Geary, A. Vetri, A. Roque, D. Furones, A. Garden, P. Orozova, I. Arzul, M. Sicard, G. M. Charrière, D. Destoumieux-Garzón, M.-A. Travers, Emergence and clonal expansion of Vibrio aestuarianus lineages pathogenic for oysters in Europe. *Mol. Ecol.* **32**, 2869–2883 (2023).
33. P. Schmitt, R. Rosa, M. Duperthuy, J. de Lorgeril, E. Bachère, D. Destoumieux-Garzon, The Antimicrobial Defense of the Pacific Oyster, Crassostrea gigas. How Diversity may Compensate for Scarcity in the Regulation of Resident/Pathogenic Microflora. *Front. Microbiol.* **3** (2012).
34. G. Vogt, Hidden Treasures in Stem Cells of Indeterminately Growing Bilaterian Invertebrates. *Stem Cell Rev. Rep.* **8**, 305–317 (2012).
35. M. Jemaà, N. Morin, P. Cavelier, J. Cau, J. M. Strub, C. Delsert, Adult somatic progenitor cells and hematopoiesis in oysters. *J. Exp. Biol.* **217**, 3067–3077 (2014).
36. S. P. Fahl, M. Wang, Y. Zhang, A.-C. E. Duc, D. L. Wiest, Regulatory Roles of Rpl22 in Hematopoiesis: An

Old Dog with New Tricks. *Crit. Rev. Immunol.* **35**, 379–400 (2015).
37. L. Jarzebowski, M. Le Bouteiller, S. Coqueran, A. Raveux, S. Vandormael-Pournin, A. David, A. Cumano, M. Cohen-Tannoudji, Mouse adult hematopoietic stem cells actively synthesize ribosomal RNA. *RNA* **24**, 1803–1812 (2018).
38. M. Rehn, A. Wenzel, A.-K. Frank, M. B. Schuster, S. Pundhir, N. Jørgensen, K. Vitting-Seerup, Y. Ge, J. Jendholm, M. Michaut, E. M. Schoof, T. L. Jensen, N. Rapin, R. T. Sapio, K. L. Andersen, A. H. Lund, M. Solimena, M. Holzenberger, D. G. Pestov, B. T. Porse, PTBP1 promotes hematopoietic stem cell maintenance and red blood cell development by ensuring sufficient availability of ribosomal constituents. *Cell Rep.* **39**, 110793 (2022).
39. J. Cao, M. Spielmann, X. Qiu, X. Huang, D. M. Ibrahim, A. J. Hill, F. Zhang, S. Mundlos, L. Christiansen, F. J. Steemers, C. Trapnell, J. Shendure, The single-cell transcriptional landscape of mammalian organogenesis. *Nature* **566**, 496–502 (2019).
40. D. Hultmark, I. Andó, Hematopoietic plasticity mapped in Drosophila and other insects. *eLife* **11**, e78906 (2022).
41. U. Banerjee, J. R. Girard, L. M. Goins, C. M. Spratford, Drosophila as a Genetic Model for Hematopoiesis. *Genetics* **211**, 367–417 (2019).
42. E. Boada-Romero, J. Martinez, B. L. Heckmann, D. R. Green, The clearance of dead cells by efferocytosis. *Nat. Rev. Mol. Cell Biol.* **21**, 398–414 (2020).
43. D. C. Dale, L. Boxer, W. C. Liles, The phagocytes: neutrophils and monocytes. *Blood* **112**, 935–945 (2008).
44. T. Rubio, D. Oyanedel, Y. Labreuche, E. Toulza, X. Luo, M. Bruto, C. Chaparro, M. Torres, J. de Lorgeril, P. Haffner, J. Vidal-Dupiol, A. Lagorce, B. Petton, G. Mitta, A. Jacq, F. Le Roux, G. M. Charrière, D. Destoumieux-Garzón, Species-specific mechanisms of cytotoxicity toward immune cells determine the successful outcome of Vibrio infections. *Proc. Natl. Acad. Sci.* **116**, 14238–14247 (2019).
45. A. S. Vanhove, T. P. Rubio, A. N. Nguyen, A. Lemire, D. Roche, J. Nicod, A. Vergnes, A. C. Poirier, E. Disconzi, E. Bachère, F. Le Roux, A. Jacq, G. M. Charrière, D. Destoumieux-Garzón, Copper homeostasis at the host vibrio interface: lessons from intracellular vibrio transcriptomics. *Environ. Microbiol.* **18**, 875–888 (2016).
46. A. C. Poirier, P. Schmitt, R. D. Rosa, A. S. Vanhove, S. Kieffer-Jaquinod, T. P. Rubio, G. M. Charrière, D. Destoumieux-Garzón, Antimicrobial Histones and DNA Traps in Invertebrate Immunity. *J. Biol. Chem.* **289**, 24821–24831 (2014).
47. A. C. Poirier, P. Schmitt, R. D. Rosa, A. S. Vanhove, S. Kieffer-Jaquinod, T. P. Rubio, G. M. Charrière, D. Destoumieux-Garzón, Antimicrobial Histones and DNA Traps in Invertebrate Immunity: Evidences in Crassostrea Gigas *. *J. Biol. Chem.* **289**, 24821–24831 (2014).
48. G. Zaroogian, P. Yevich, Cytology and biochemistry of brown cells in *Crassostrea virginica* collected at clean and contaminated stations. *Environ. Pollut.* **79**, 191–197 (1993).
49. B. Allam, D. Raftos, Immune responses to infectious diseases in bivalves. *J. Invertebr. Pathol.* **131**, 121–136 (2015).
50. J. Nakhleh, L. El Moussawi, M. A. Osta, "Chapter Three - The Melanization Response in Insect Immunity" in *Advances in Insect Physiology*, P. Ligoxygakis, Ed. (Academic Press, 2017; https://www.sciencedirect.com/science/article/pii/S0065280616300467)vol. 52 of *Insect Immunity*, pp. 83–109.
51. P. Amparyup, W. Charoensapsri, A. Tassanakajon, Prophenoloxidase system and its role in shrimp immune responses against major pathogens. *Fish Shellfish Immunol.* **34**, 990–1001 (2013).
52. S. Picot, N. Faury, C. Pelletier, I. Arzul, B. Chollet, L. Dégremont, T. Renault, B. Morga, Monitoring Autophagy at Cellular and Molecular Level in Crassostrea gigas During an Experimental Ostreid Herpesvirus 1 (OsHV-1) Infection. *Front. Cell. Infect. Microbiol.* **12** (2022).
53. N. R. de la Ballina, A. Villalba, A. Cao, Differences in proteomic profile between two haemocyte types, granulocytes and hyalinocytes, of the flat oyster *Ostrea edulis*. *Fish Shellfish Immunol.* **100**, 456–466 (2020).
54. S. Aladaileh, S. V. Nair, D. Birch, D. A. Raftos, Sydney rock oyster (*Saccostrea glomerata*) hemocytes: Morphology and function. *J. Invertebr. Pathol.* **96**, 48–63 (2007).
55. E. Rifkin, T. C. Cheng, H. R. Hohl, An electron-microscope study of the constituents of encapsulating cysts in the American oyster, *Crassostrea virginica*, formed in response to *Tylocephalum* metacestodes. *J. Invertebr. Pathol.* **14**, 211–226 (1969).
56. N. De San Nicolas, A. Asokan, R. D. Rosa, S. N. Voisin, M.-A. Travers, G. Rocha, L. Dantan, Y. Dorant, G. Mitta, B. Petton, G. M. Charrière, J.-M. Escoubas, V. Boulo, J. Pouzadoux, H. Meudal, K. Loth, V. Aucagne, A. F. Delmas, P. Bulet, C. Montagnani, D. Destoumieux-Garzón, Functional Diversification of Oyster Big Defensins Generates Antimicrobial Specificity and Synergy against Members of the Microbiota. *Mar. Drugs* **20**, 745 (2022).
57. N. R. de la Ballina, A. Villalba, A. Cao, Shotgun analysis to identify differences in protein expression between granulocytes and hyalinocytes of the European flat oyster Ostrea edulis. *Fish Shellfish Immunol.* **119**, 678–691 (2021).
58. J. de Lorgeril, A. Lucasson, B. Petton, E. Toulza, C. Montagnani, C. Clerissi, J. Vidal-Dupiol, C. Chaparro, R.

Galinier, J.-M. Escoubas, P. Haffner, L. Dégremont, G. M. Charrière, M. Lafont, A. Delort, A. Vergnes, M. Chiarello, N. Faury, T. Rubio, M. A. Leroy, A. Pérignon, D. Régler, B. Morga, M. Alunno-Bruscia, P. Boudry, F. Le Roux, D. Destoumieux-Garzón, Y. Gueguen, G. Mitta, Immune-suppression by OsHV-1 viral infection causes fatal bacteraemia in Pacific oysters. *Nat. Commun.* **9**, 4215 (2018).

59. E. A. Pila, J. T. Sullivan, X. Z. Wu, J. Fang, S. P. Rudko, M. A. Gordy, P. C. Hanington, Haematopoiesis in molluscs: A review of haemocyte development and function in gastropods, cephalopods and bivalves. *Dev. Comp. Immunol.* **58**, 119–128 (2016).
60. M. de Bruijn, E. Dzierzak, Runx transcription factors in the development and function of the definitive hematopoietic system. *Blood* **129**, 2061–2069 (2017).
61. E. W. Scott, M. C. Simon, J. Anastasi, H. Singh, Requirement of transcription factor PU.1 in the development of multiple hematopoietic lineages. *Science* **265**, 1573–1577 (1994).
62. I. Bergiers, T. Andrews, Ö. Vargel Bölükbaşı, A. Buness, E. Janosz, N. Lopez-Anguita, K. Ganter, K. Kosim, C. Celen, G. Itır Perçin, P. Collier, B. Baying, V. Benes, M. Hemberg, C. Lancrin, Single-cell transcriptomics reveals a new dynamical function of transcription factors during embryonic hematopoiesis. *eLife* **7**, e29312 (2018).
63. S. F. Altschul, W. Gish, W. Miller, E. W. Myers, D. J. Lipman, Basic local alignment search tool. *J. Mol. Biol.* **215**, 403–410 (1990).
64. P. Jones, D. Binns, H.-Y. Chang, M. Fraser, W. Li, C. McAnulla, H. McWilliam, J. Maslen, A. Mitchell, G. Nuka, S. Pesseat, A. F. Quinn, A. Sangrador-Vegas, M. Scheremetjew, S.-Y. Yong, R. Lopez, S. Hunter, InterProScan 5: genome-scale protein function classification. *Bioinformatics* **30**, 1236–1240 (2014).
65. C. P. Cantalapiedra, A. Hernández-Plaza, I. Letunic, P. Bork, J. Huerta-Cepas, eggNOG-mapper v2: Functional Annotation, Orthology Assignments, and Domain Prediction at the Metagenomic Scale. *Mol. Biol. Evol.* **38**, 5825–5829 (2021).
66. S. Götz, J. M. García-Gómez, J. Terol, T. D. Williams, S. H. Nagaraj, M. J. Nueda, M. Robles, M. Talón, J. Dopazo, A. Conesa, High-throughput functional annotation and data mining with the Blast2GO suite. *Nucleic Acids Res.* **36**, 3420–3435 (2008).
67. Y. Hao, S. Hao, E. Andersen-Nissen, W. M. Mauck, S. Zheng, A. Butler, M. J. Lee, A. J. Wilk, C. Darby, M. Zager, P. Hoffman, M. Stoeckius, E. Papalexi, E. P. Mimitou, J. Jain, A. Srivastava, T. Stuart, L. M. Fleming, B. Yeung, A. J. Rogers, J. M. McElrath, C. A. Blish, R. Gottardo, P. Smibert, R. Satija, Integrated analysis of multimodal single-cell data. *Cell* **184**, 3573-3587.e29 (2021).
68. R. M. Wright, G. V. Aglyamova, E. Meyer, M. V. Matz, Gene expression associated with white syndromes in a reef building coral, Acropora hyacinthus. *BMC Genomics* **16**, 371 (2015).

Acknowledgments

We are grateful to the staff of the Ifremer platform of "La Tremblade" for technical support in animal housing. scRNA-seq data generated and used in this work were produced through the MGX platform (University of Montpellier, CNRS ,INSERM). We thank the bioinformatic service of Ifremer (SEBIMER) for their help in bioinformatics and the qPCR platform GenSeq (University of Montpellier). We would like to thank Viviane Boulo and Danielle Mello for their enriching discussions, as well as all the members of the 2MAP laboratory team for the fruitful discussions throughout this project.

Ethics

This work did not require ethical approval from a human subject or animal welfare committee.

Funding

This work was funded by the Agence Nationale de la Recherche (MOSAR-DEF, ANR-19-CE18-0025; DECICOMP, ANR-19-CE20-0004 and TRANSCAN ANR-18-CE35-0009), the University of Montpellier, iSite MUSE and the "GT-Huître" initiative from Ifremer. This study falls within the framework of the "Laboratoires d'Excellence (LABEX)" Tulip (ANR-10-LABX-41). Sébastien De La Forest Divonne was awarded a PhD grant from the Region Occitanie (HemoFight project) and the University of Perpignan Via Domitia graduate school ED305.

Author contributions

Conceptualization: G.M., D.D.-G., B.G., G.M.C. and E.V.

Methodology: S.d.L.F.D., J.P., G.M., D.D.-G., B.G., G.M.C. and E.V.

Investigation: S.d.L.F.D., J.P., G.M.C. and E.V.

Supervision: G.M.C. and E.V.

Writing (original draft): S.d.L.F.D. and E.V.

Writing (review and editing): all authors.

Competing interests

The authors declare that they have no competing interests.